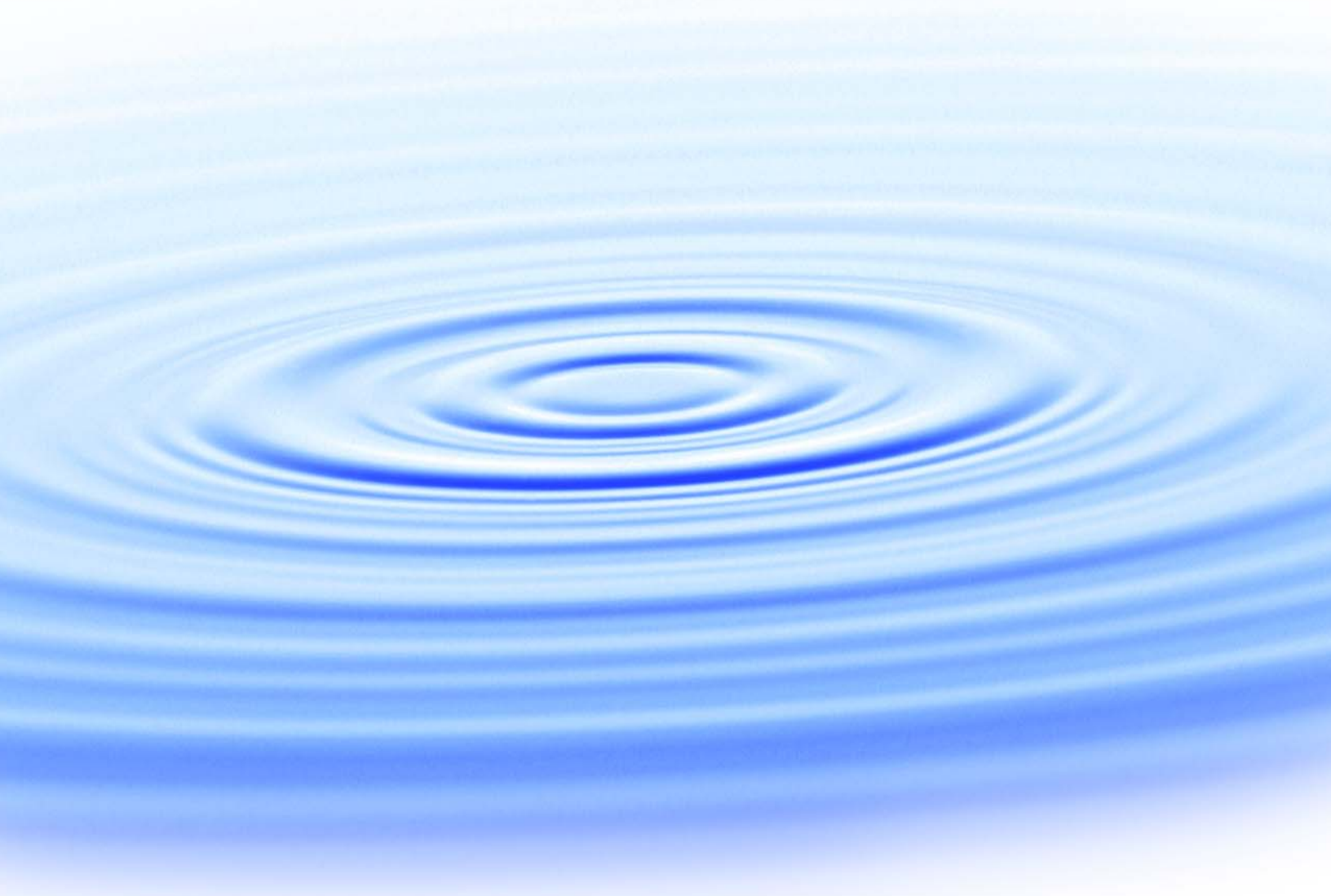




**Characterization of U.S. Seawaters and
Development of Standardized Protocols
for Evaluation of Foulants in Seawater
Reverse Osmosis Desalination**



Characterization of U.S. Seawaters and
Development of Standardized Protocols for
Evaluation of Foulants in Seawater Reverse
Osmosis Desalination

About the WaterReuse Research Foundation

The mission of the WaterReuse Research Foundation is to conduct and promote applied research on the reclamation, recycling, reuse, and desalination of water. The Foundation's research advances the science of water reuse and supports communities across the United States and abroad in their efforts to create new sources of high quality water through reclamation, recycling, reuse, and desalination while protecting public health and the environment.

The Foundation sponsors research on all aspects of water reuse, including emerging chemical contaminants, microbiological agents, treatment technologies, salinity management and desalination, public perception and acceptance, economics, and marketing. The Foundation's research informs the public of the safety of reclaimed water and provides water professionals with the tools and knowledge to meet their commitment of increasing reliability and quality.

The Foundation's funding partners include the Bureau of Reclamation, the California State Water Resources Control Board, the California Energy Commission, and the California Department of Water Resources. Funding is also provided by the Foundation's Subscribers, water and wastewater agencies, and other interested organizations.

Characterization of U.S. Seawaters and Development of Standardized Protocols for Evaluation of Foulants in Seawater Reverse Osmosis Desalination

Samer Adham, Ph.D.
MWH

Mark Clark, Ph.D.
University of Illinois, Urbana-Champaign

Cosponsor

Bureau of Reclamation



WaterReuse Research Foundation
Alexandria, VA

Disclaimer

This report was sponsored by the WateReuse Research Foundation and cosponsored by the Bureau of Reclamation. The Foundation, its Board Members, and the project cosponsors assume no responsibility for the content of this publication or for the opinions or statements of facts expressed in the report. The mention of trade names of commercial products does not represent or imply the approval or endorsement of the WateReuse Research Foundation, its Board Members, or the cosponsors. This report is published solely for informational purposes.

For more information, contact:

WateReuse Research Foundation
1199 North Fairfax Street, Suite 410
Alexandria, VA 22314
703-548-0880
703-548-5085 (fax)
www.WateReuse.org/Foundation

© Copyright 2011 by the WateReuse Research Foundation. All rights reserved. Permission to reproduce must be obtained from the WateReuse Research Foundation.

WateReuse Research Foundation Project Number: WRF-06-014
WateReuse Research Foundation Product Number: 06-014-1

ISBN: 978-1-934183-47-2
Library of Congress Control Number: 2011944528

Printed in the United States of America

Printed on Recycled Paper

Contents

List of Figures.....	vii
List of Tables	ix
Acronyms and Abbreviations	x
Foreword.....	xiii
Acknowledgments	xiv
Executive Summary.....	xv
Chapter 1. Introduction.....	1
1.1. Background	1
1.2. Objectives.....	3
Chapter 2. Materials and Methods.....	5
2.1. Feed Water Source Selection and Characterization	5
2.1.1. Basic Water Quality Analysis.....	5
2.1.2. Size Distribution of Organic Matter.....	6
2.2. Membrane Selection and Characterization	6
2.2.1. Surface Potential	6
2.2.2. Surface Roughness	7
2.2.3. Contact Angle Analysis	8
2.2.4. Surface Functionality	8
2.2.5. Surface Morphology	9
2.3. Foulant Characterization	9
2.4. Bench-Scale Testing.....	10
2.4.1. Equilibration Study	12
2.4.2. Seawater Fouling Study	12
2.4.3. AOM Fouling Study.....	12
2.5. Pilot-Scale Element Autopsy	12
2.6. Surface Energy Analysis.....	12
Chapter 3. Results and Discussion	15
3.1. Feed Water Characteristics	15
3.2. Clean Membrane Characteristics	17
3.2.1. Surface Morphology using SEM.....	17
3.2.2. Surface Charge using Streaming Potential Measurements	19
3.2.3. Surface Roughness using AFM.....	20
3.2.4. Surface Hydrophobicity using Contact Angle Measurements	22
3.3. Bench-Scale Testing of Different Seawater Sources	24
3.3.1. Foulant Analysis of West Basin Seawater	26

3.3.2. Foulant Analysis of Tampa Bay Seawater.....	29
3.3.3. Foulant Analysis of Carlsbad Seawater.....	31
3.3.4. Determination of Surface Energy of Foulant Layer	35
3.4. Impact of Membrane Type on Fouling.....	37
3.5. Impact of AOM Fouling.....	38
3.6. Comparison of Bench-Scale and Pilot-Scale Fouling.....	47
3.7. Applicability of Analytical Methods for SWRO Processes.....	50
Chapter 4. Conclusions and Recommendations	57
4.1. Conclusions	57
4.2. Recommended Future Work.....	59
4.3. Practical Aspects of the Study	59
References	61
Appendix A	65

Figures

2.1	Electrical double layer formed at the membrane surface.....	7
2.2	Illustration of ATR principle	9
2.3	Illustration of foulant characterization techniques.....	10
2.4	Schematic of bench-scale experimental setup	11
2.5	Picture of bench-scale experimental setup.....	11
3.1	Measured carbohydrate concentrations for the various seawater sources.	17
3.2	SEM images of clean Hydranautics SWC4, Saehan SR, and DowFilmtec SW30HR membranes	18
3.3	SEM images of the Saehan SR membrane at 50,000× and 75,000× magnifications.....	19
3.4	Zeta potential as a function of pH and ionic strength for the model membranes	20
3.5	AFM topographs for different commercial dried virgin membranes.....	21
3.6	Images of DI water droplets on model membranes	22
3.7	Comparison of contact angles using 3 liquids on model SWRO membranes	23
3.8	Normalized specific flux for all 3 seawater sources for studies conducted with Hydranautics SWC4 membranes performed at UIUC and MWH.....	25
3.9	SEM image of Hydranautics SWC4 membrane fouled by West Basin seawater.....	26
3.10	EDS analysis of Hydranautics SWC4 membrane fouled with West Basin seawater.	27
3.11	AFM topograph of Hydranautics SWC4 membrane fouled with West Basin seawater and roughness parameters.....	28
3.12	ATR-FTIR spectra from the fouled Hydranautics membrane coupon run with West Basin seawater at UIUC.....	28
3.13	SEM image of Hydranautics SWC4 membrane fouled by Tampa Bay seawater.....	29
3.14	EDS analysis of Tampa Bay seawater-fouled Hydranautics SWC4 membranes	30
3.15	AFM topograph of Hydranautics SWC4 membrane fouled with Tampa Bay seawater and roughness parameters.	30
3.16	ATR-FTIR spectra from the fouled membrane coupon run with Tampa Bay seawater at UIUC.....	31
3.17	SEM image of Carlsbad-fouled Hydranautics SWC4 membrane (MWH sample).	31
3.18	EDS analysis of Carlsbad-fouled Hydranautics SWC4 membrane (MWH sample).....	32
3.19	SEM image of Carlsbad-fouled Hydranautics SWC4 membrane (UIUC sample).....	33

3.20	EDS analysis of Carlsbad-fouled Hydranautics SWC4 membrane (UIUC sample)	34
3.21	ATR-FTIR spectra from the fouled membrane coupon run with Carlsbad seawater at UIUC	34
3.22	ATR-FTIR spectra from the fouled membrane coupon run with Carlsbad seawater at MWH.....	35
3.23	Comparison of contact angles using 3 liquids on fouled Hydranautics SWC4 membrane	35
3.24	Illustration of interaction between seawater foulant and clean/modified membrane	36
3.25	Comparison of normalized specific flux for Hydranautics SWC4 and DowFilmtec SW30HR membranes with South Bay seawater.	37
3.26	SEM images of <i>H. pygmaea</i> cells.....	39
3.27	Normalized specific flux decline comparison for Hydranautics SWC4 and DowFilmtec SW30HR membranes with <i>H. pygmaea</i> cells with no prefiltration.....	40
3.28.	Normalized specific flux decline comparison for Hydranautics SWC4 and DowFilmtec SW30HR membranes with <i>H. pygmaea</i> cells with pre-MF	40
3.29	Digital images of fouled Hydranautics SWC4 membrane when <i>H. pygmaea</i> -spiked water was used without prefiltration.	41
3.30	SEM images of fouled Hydranautics SWC4 membrane at 600×, 3000×, and 10,000× magnifications when <i>H. pygmaea</i> -spiked water was used without prefiltration	42
3.31	Images of fouled Hydranautics SWC4 membrane when <i>H. pygmaea</i> -spiked water was used with pre-MF.	43
3.32	SEM images of AOM fouling on Hydranautics SWC4 membrane coupon at 600×, 3000×, and 10,000× magnification.	44
3.33	SEM image of DowFilmtec SW30HR membrane after AOM fouling experiment. Locations A and B were chosen for EDS analysis.	45
3.34	EDS spectrum at location A in the SEM image shown in Figure 3.33.	46
3.35	EDS spectrum at location B in the SEM image shown in Figure 3.33.....	46
3.36	Infrared absorbance spectra in the region of 3700 to 2600 cm ⁻¹ for Hydranautics SWC4 (solid line) and DowFilmtec (dashed line) after experiments with <i>H. pygmaea</i> water with/without prefiltration.....	47
3.37	SEM image of lead element from the Carlsbad pilot plant	48
3.38	EDS analysis of lead element from the Carlsbad pilot plant.....	49
3.39	ATR-FTIR spectra from the autopsy of a Hydranautics SWC4+ membrane module used in the Carlsbad seawater desalination pilot facility.....	50
3.40	Steps to analyze organic fouling potential of different seawater sources.....	53

Tables

2.1	Analytical Methods Used for Seawater Characterization	6
3.1	Chemistry of Various Seawater Sources.....	16
3.2	Roughness Parameters for Clean Membranes	21
3.3	Surface Energy Parameters (mJ/m ²) for Clean SWRO Membranes.....	24
3.4	Surface Energy Parameters (mJ/m ²) for Fouled Hydraulics SWC4 Membrane	36
3.5	Summary of Analytical Methods Used for Characterization of Seawater, Membrane, and Foulant.....	54

Acronyms and Abbreviations

AFM	atomic force microscopy
AOM	algogenic organic matter
ATR-FTIR	attenuated total reflectance-fourier transform infrared
CDP	Carlsbad Desalination Project
DI	deionized
DOC	dissolved organic carbon
EDS	energy dispersive spectroscopy
FTIR	fourier transform infrared spectroscopy
gfd	gallons per square feet per day
HPSEC	high-performance size exclusion chromatography
ICP	ion-coupled plasma
IRE	internal reflection element
LOI	loss on ignition
MF	microfiltration
mM	millimolar
MWH	Montgomery Watson Harza
PA	polyamide
RO	reverse osmosis
RMS	root mean square
SAD	surface area difference
SBPP	South Bay Power Plant
SDI	silt density index
(SDI) ₁₅	silt density index – 15 min
SEM	scanning electron microscopy
SWRO	seawater reverse osmosis
TBDP	Tampa Bay Desalination Plant
TDS	total dissolved solids
TEP	transparent exopolymers
TFC	thin film composite
TOC	total organic carbon
UF	ultrafiltration
UIUC	University of Illinois–Urbana-Champaign
WBMWD	West Basin Municipal Water District
γ	surface energy, mJ/m ²
θ	contact angle, deg
ΔG	free energy, mJ/m ²

Subscripts

<i>s</i>	solid
<i>l</i>	liquid
<i>c</i>	colloid
<i>h_o</i>	at contact (0.158 nm)

Superscripts

<i>LW</i>	Lifshitz–van der Waals
<i>AB</i>	acid–base
+	electron-acceptor
-	electron-donor

Foreword

The WateReuse Research Foundation, a nonprofit corporation, sponsors research that advances the science of water reclamation, recycling, reuse, and desalination. The Foundation funds projects that meet the water reuse and desalination research needs of water and wastewater agencies and the public. The goal of the Foundation's research is to ensure that water reuse and desalination projects provide high-quality water, protect public health, and improve the environment.

An Operating Plan guides the Foundation's research program. Under the plan, a research agenda of high-priority topics is maintained. The agenda is developed in cooperation with the water reuse and desalination communities including water professionals, academics, and Foundation subscribers. The Foundation's research focuses on a broad range of water reuse research topics including:

- Defining and addressing of emerging contaminants
- Public perceptions of the benefits and risks of water reuse
- Management practices related to indirect potable reuse
- Groundwater recharge and aquifer storage and recovery
- Evaluation and methods for managing salinity and desalination
- Economics and marketing of water reuse

The Operating Plan outlines the role of the Foundation's Research Advisory Committee (RAC), project advisory committees (PACs), and Foundation staff. The RAC sets priorities, recommends projects for funding, and provides advice and recommendations on the Foundation's research agenda and other related efforts. PACs are convened for each project and provide technical review and oversight. The Foundation's RAC and PACs consist of experts in their fields and provide the Foundation with an independent review, which ensures the credibility of the Foundation's research results. The Foundation's Project Managers facilitate the efforts of the RAC and PACs and provide overall management of projects.

The Foundation's primary funding partners include the Bureau of Reclamation, California State Water Resources Control Board, the California Energy Commission, Foundation Subscribers, water and wastewater agencies, and other interested organizations. The Foundation leverages its financial and intellectual capital through these partnerships and other funding relationships.

Desalination technologies using reverse osmosis membranes have been in development for more than four decades. In this study, a systematic approach to study organic fouling and determine the key foulants depositing on the membrane surface is presented. This study characterizes seawater from various locations in the United States and evaluates methods for characterizing clean and fouled membranes.

Joseph Jacangelo
Chair
WateReuse Research Foundation

G. Wade Miller
Executive Director
WateReuse Research Foundation

Acknowledgments

This project was funded by the WateReuse Research Foundation in cooperation with the Bureau of Reclamation. This study would not have been possible without the insights, efforts, and dedication of many individuals and organizations. These include the members of the research team; project advisory committee (PAC) members; and the WateReuse Research Foundation's project manager, Anna Durden.

The research team thanks the WateReuse Research Foundation and Bureau of Reclamation for funding this project, as well as the following organizations for providing assistance during the course of the project: West Basin Municipal Water District, Poseidon Resources, Tampa Bay Water, and University of California, Los Angeles. The project team also thanks Dan Marler (Carlsbad Desalination Project), Monica Tirtadidjaja (West Basin Municipal Water District), John Troutt (Tampa Bay Water), Tom Lids (South Bay Power Plant), Zakir Hirani (MWH), and Eric Bruce (MWH) for assisting in seawater sampling. Thanks to Paige Gourley and Rich Franks from Hydranautics for providing pilot plant element for autopsy. Sincere thanks to the personnel of MWH, especially Joan Oppenheimer, Geno Lehman, and Li Liu, for proofreading the report.

Principal Investigator

Samer Adham, Ph.D., *MWH*

Co-Principal Investigator

Mark Clark, Ph.D., *University of Illinois, Urbana-Champaign*

Research Project Team

Arun Subramani, Ph.D., *MWH*

Mohammad Badruzzaman, Ph.D., P.E., *MWH*

David Ladner, Ph.D., *University of Illinois, Urbana-Champaign*

Manish Kumar, P.E., *University of Illinois, Urbana-Champaign*

Project Advisory Committee

Eric Hoek, Ph.D., *University of California, Los Angeles*

Donald Polmann, Ph.D., P.E., *Tampa Bay Water*

Phil Lauri, *West Basin Municipal Water District*

Nikolay Voutchkov, *Water Globe Consulting LLC*

Steven Dundorf, *Bureau of Reclamation*

Executive Summary

Desalination technologies using reverse osmosis (RO) membranes have been in development for more than four decades. Although significant advances in membrane technology have been developed to efficiently operate seawater RO (SWRO) systems, control of membrane fouling still seems elusive. Fouling in SWRO systems has been reported to occur because of the presence of colloids, microorganisms, and organics present in the seawater (Wilf and Klinko, 1998). Because of seawater's complex matrix, characterization and identification of the nature of foulants responsible for decreased SWRO performance are incomplete.

In this study, a systematic approach to study organic fouling and determine the key foulants depositing on the membrane surface is presented. The objectives of the study were to characterize seawater from various locations in the United States, evaluate methods for characterizing clean and fouled membranes, identify organic foulants using bench-scale RO experiments, study the influence of membrane properties and algal bloom (red-tide events) on organic fouling, and compare fouling between bench-scale SWRO operation and pilot-scale SWRO operation.

Seawater from West Basin Municipal Water District (WBMWD), Carlsbad Desalination Project (CDP), Tampa Bay Desalination Plant (TBDP), and South Bay Power Plant (SBPP) was chosen as the feed water sources for this study. Membranes used in the study were DowFilmtec SW30HR, Hydranautics SWC4, and Saehan SR. To test the different seawaters for fouling propensity, a bench-scale RO unit was constructed at MWH in California and University of Illinois, Urbana-Champaign (UIUC). Experimental results and evaluation of methods for determining organic fouling in seawater are presented in detail in this study.

To characterize the raw seawater, analytical techniques included determination of major ions, total organic carbon (TOC), and polysaccharide content. Major ions were determined by standard methods using appropriate dilutions. TOC was determined using an UV/persulfate analyzer, and polysaccharide content was determined using absorbance at 595 nm. In order to identify the major foulant depositing on the membrane surface, bench-scale experiments were conducted with a SEPA[®] cell. Rapid bench-scale experiments were conducted for a period of 24 h under hydrodynamic conditions similar to those existing in spiral-wound elements. The membrane coupons from bench-scale experiments were removed after the fouling study, and various autopsy techniques were performed to identify the nature of foulant deposited. Attenuated total reflectance-Fourier transform infrared spectroscopy was used to quantify the organic content of the foulant layer. Scanning electron microscopy, atomic force microscopy, and energy dispersive spectroscopy were used to determine the surface morphology (before/after fouling) and inorganic constituents of the foulant layer. To determine the hydrophobic/hydrophilic nature of the foulant layer, contact angle analyses using one apolar and two polar liquids were used. Studies were also performed to determine the influence of membrane surface properties (surface charge, roughness, and hydrophobicity) on fouling. The characteristic brick-redness of most red tides is due to photosynthetic pigments of dinoflagellates. To determine the influence of an algal bloom on fouling behavior, algogenic organic matter from the cells of a marine bloom-forming dinoflagellate, *Heterocapsa pygmaea*, was used to conduct fouling experiments.

Seawater characterization results showed that the concentrations of major ions in all the seawater sources were similar. Total dissolved solid (TDS) concentrations were in the range

of 31,000–33,600 mg/L, and pH was between 7.8 and 8.0. Silt density index – 15 min was higher (~6.3) for Tampa Bay seawater than for the other sources. Chloride and sodium were the major ions present in all sources. Among the divalent ions, magnesium concentration was significantly higher than calcium's. Concentrations of major metals (iron, aluminum, nickel, and copper) were below detection limits in all the raw seawater sources. Carbohydrate concentration of Tampa Bay seawater was higher than for seawater from Carlsbad, West Basin, and South Bay. Also, TOC concentration was highest for Tampa Bay (~2.5 mg/L). TOC concentrations for all the other sources were below the lowest detection limit.

Clean membrane characterization results revealed that DowFilmtec SW30HR and Saehan SR membranes were relatively smooth (root mean square [RMS] roughness ~ 78 nm) when compared to Hydranautics SWC4 (RMS roughness ~ 150 nm). DowFilmtec SW30HR membrane was relatively hydrophilic compared to Hydranautics SWC4 and Saehan SR membranes. Streaming potential measurements were not significantly different for the membranes at ionic strengths greater than 100 mM and pH = 8.0.

When bench-scale RO experiments were performed with all the source seawaters, no significant difference in normalized specific flux was observed. Hence, no correlation between seawater quality and fouling propensity could be made based only on flux decline results. Membrane properties seemed to play a role in foulant deposition when seawater was used. Relatively smooth and hydrophilic membrane (DowFilmtec SW30HR) exhibited slightly lower decline in specific flux than did relatively rough and hydrophobic membrane (Hydranautics SWC4). When AOM was used without any pretreatment of feed water, a gel layer was formed on the membrane surface. But with premicrofiltration (pre-MF), nonuniform deposition occurred on the membrane surface. Hence, pre-MF reduced the AOM content reaching the SWRO membrane. Although a minimal decline in specific flux of the SWRO membrane was noticed with pre-MF, deposition of foulant was evident from autopsy techniques.

Polysaccharide-like material was identified as a major part of the foulant layer for all the seawater sources. The nature of foulant was similar both in rapid bench-scale studies and in a lead SWRO element from a pilot plant. In both bench-scale and pilot-scale evaluation, corrosion products were found to be deposited on the membrane surface. Because of the short experimental period in the bench-scale studies, uniform coverage of the foulant layer was not attained. But in the pilot plant element, a thick slimy cake layer consisting of protein-like and polysaccharide-like material was identified.

The techniques and methods used in this study can be used prior to the operation of a pilot-scale process in order to access the nature of foulant material that would preferentially deposit on the membrane surface. The bench-scale experiments must be combined with the various analyses, characterizations, and autopsy techniques described in this study to obtain meaningful results. An understanding of the nature of foulant will facilitate cost-effective and optimal design/operation of pretreatment and the overall SWRO process.

Chapter 1

Introduction

1.1 BACKGROUND

Seawater desalination technology has been gaining acceptance for the production of additional freshwater because of scarcity of freshwater, technology development, and reduced costs. As of 2005, more than 15,000 seawater desalination facilities operated in more than 120 countries worldwide (Voutchkov, 2005). The main drawback associated with membrane processes is fouling on the membrane surface, which leads to decreased productivity and increased operating costs from the higher applied pressure requirements and membrane cleaning costs. Although a number of seawater reverse osmosis (SWRO) facilities are in operation, there is limited understanding of the key components responsible for fouling. A fundamental understanding of the nature of major foulants in seawater desalination is needed in order to further optimize the SWRO process and reduce the energy and chemical requirements for efficient operation.

Fouling in SWRO systems has been reported to be primarily due to the presence of colloidal and particulate matter, dissolved organics, and biological growth within the RO system (Wilf and Klinko, 1998). Precipitation of sparingly soluble salts (scaling) is less of a concern in the SWRO process because of the low recovery (typically 40–50%) and low concentration of bicarbonate ion. Transport of particulates and organic macromolecules towards the membrane surface is influenced by permeate drag forces acting perpendicular to the membrane surface. Once the particulates, colloids, and organic matter are transported to the membrane surface, a foulant layer is formed. In seawater, higher fouling rates have been reported to occur at a relatively low permeate flux (6–8 gal per sq foot per day [gfd]). Because of high ionic strength, electrostatic repulsive forces are suppressed, leading to a higher fouling rate at a lower flux (Wilf and Klinko, 1998). Colloidal and organic deposition occurs gradually, and fouling can be reduced by the type of pretreatment employed. Although cleaning strategies exist to recover the specific flux to initial value after fouling, loss of productivity due to system shutdown is a disadvantage.

Design and operation of SWRO plants are strongly dependent on the raw water quality (Leparc et al., 2007; Glueckstern et al., 2002; Isias, 2001; Al-Ahmad et al., 2000; Reiss et al., 2008). Seawater intake is either from an open surface, subsurface, or a well (Wilf and Klinko, 1998). Past studies have determined that the turbidity, total organic carbon (TOC), bacteria, and chlorophyll concentrations were significantly lower for well seawater than for surface intake sources (Leparc et al., 2007). Silt density index – 15 min (SDI)₁₅ values were < 3 for well water, whereas (SDI)₁₅ values were ~ 6 for open intake. TOC values for well water were significantly different from those for open intake. Membrane manufacturers and utilities rely on the SDI as a parameter for predicting fouling in SWRO systems. One limitation of the method is the use of a 0.45- μ m-pore-size filter in a dead-end filtration mode, whereas RO processes use crossflow velocity. Hence, the nature of foulants in SDI testing will not accurately represent the RO foulants. Modifications to SDI measurements have recently been developed to utilize a crossflow fouling sampler index (Adham and Fane, 2008), but the technology is still under development.

Pretreatment of seawater is critical for proper operation of SWRO systems. Conventional pretreatment using flocculation, coagulation, and multimediuim filtration is widely being used to reduce the SDI and remove excessive turbidity and suspended solids. However, conventional pretreatment may not provide a complete barrier to colloids and suspended particles and also produces variable feed water quality (Brehant et al., 2002). Hence, microfiltration (MF) and ultrafiltration (UF) have become attractive pretreatment alternatives (Wilf and Klinko, 1999; Brehant et al., 2002). In one study, bench-scale experiments were performed to study the influence of different pretreatment types on SWRO fouling (Kumar et al., 2006). It was found that particulate matter greater than 1 μm in diameter (representing conventional pretreatment) caused most of the fouling. When MF and UF membranes were used as pretreatment, fouling was significantly lower than found in conventional pretreatment but no difference in flux decline was observed between MF and UF. Lowest SWRO flux decline was observed when a tight UF membrane (20 kDa) was used as pretreatment, but a decrease in specific flux was still observed. Another study compared pilot water quality from MF and UF membranes and found that the water quality was better with UF pretreatment (Teng et al., 2003). A recent study compared MF, UF, ferric chloride (FeCl_3) flocculation, and powdered activated carbon (Shon et al., 2007). Molecular weight peaks for the seawater (southwestern Korea) used consisted of 1200 Da (biopolymers), 950 Da (fulvic acids), 650 Da (hydrolysates of humic substances), 250 Da (low-molecular-weight acids), and 90 Da (low-molecular-weight neutrals and amphiphilics). Coagulation with FeCl_3 was found to preferentially remove biopolymers, whereas PAC adsorption mostly removed fulvic acids. Prefiltration with MF and UF removed only small amounts of large dissolved organics. Also, it was found that only biopolymers were preferentially deposited on the RO membrane.

Problems that are due to biofouling in SWRO systems have also been reported to be of concern (Al-Ahmad et al., 2000). Severe increase in the applied pressure, higher decline in flux, and elevated permeate conductivity were reported to be caused by biofouling (Saeed et al., 2000; Winters, 1994; Veza et al., 2008). Biofouling was reported to be more critical when feed water temperature was above 25 $^{\circ}\text{C}$. In one study, fluidized bed biological granular activated carbon systems were found to be effective in reducing the dissolved organic carbon (DOC) concentration in feed seawater and reducing biofouling potential (Visvanathan et al., 2002).

In order to identify the major foulant responsible in SWRO systems, autopsies of fouled membranes removed from either pilot or full-scale plants have been performed. Autopsies of SWRO pilot plant elements were performed utilizing an element wet test for water flow and salt rejection determination, a dye/Fujiwara test for oxidant uptake, inductively coupled plasma emission spectroscopy for metal analysis, loss on ignition for inorganic versus organic content, and attenuated total reflection–Fourier transform infrared (ATR-FTIR) spectroscopy and protein/carbohydrate analysis for organic content (Lozier et al., 2007). Such analyses indicated that pretreatment with conventional treatment techniques resulted in greater particulate, inorganic, and organic fouling than did pretreatment using MF/UF membranes.

Other studies of fouling that is due to dissolved organic matter found that a mixture of aliphatic and aromatic compounds constitutes the total organics in seawater (Watkins and Gupta, 1987; Ghani et al., 2000). Seawater humic substances from three different locations in the Middle East were isolated and analyzed using UV-visible, infrared (IR), and fluorescence spectrometry. Due to organic fouling, excessive loss of productivity and salt rejection were experienced. Humics were reported to cause decline in specific flux in SWRO processes when flux rates were greater than 10 gfd and when cationic polymers were used for pretreatment (Winters, 1987). Humic substances are relatively stable in seawater because of

their polyanionic characteristic and ability to form hydrogen bonds with water molecules. Humics in seawater are produced by algae and bacteria through photosynthetic pathways. In seawater, the presence of polysaccharides and transparent exopolymers (TEPs) exuded by phytoplankton and bacteria can also lead to the transformation of dissolved organic matter into particulate form (Villacorte et al., 2009). Moreover, polysaccharides produced from phytoplankton and bacteria in seawater were reported to be present in high abundance (Allredge et al., 1993).

It is difficult to control organic fouling in RO processes even when various pretreatment techniques are implemented. Organic fouling in SWRO processes becomes even more complex because of the high ionic strength and suppression of repulsive electrostatic interactions. Moreover, in the event of an algal bloom, the organic loading in seawater increases dramatically because of higher microbiological activity, therefore applying shock loads to the pretreatment processes. Most of the techniques used to identify the key foulants responsible for SWRO fouling have involved running pilot plants and monitoring feed/permeate water quality along with final autopsies of fouled membrane surfaces. Although pilot plant operation is useful in determining performance parameters in conjunction with full-scale operation, identification of the nature of foulants requires considerable time. Hence, a rapid testing method to determine the major foulants in seawater is desired.

1.2. OBJECTIVES

Specific objectives of the study are as follows:

- Characterization of seawater from various sources in the United States.
- Evaluation of methods for characterizing clean and fouled membranes.
- Identification of key foulants deposited on SWRO membranes using bench-scale experiments.
- Study of the influence of algal bloom on organic fouling.

Chapter 2

Materials and Methods

2.1 FEED WATER SOURCE SELECTION AND CHARACTERIZATION

Seawater samples from West Basin Municipal Water District (WBMWD), Carlsbad Desalination Project (CDP), Tampa Bay Desalination Plant (TBDP), and South Bay Power Plant (SBPP) were chosen as the feed water sources for this study. Samples from WBMWD and CDP were collected from a feed water sampling port at the pilot plant. Samples from SBPP were collected from an open seawater intake pond feeding water to the power plant. Samples from TBDP were collected from a feed water sampling port at the full-scale plant. Three of the source seawaters (WBMWD, CDP, and SBPP) are located in California, whereas TBDP is located in Florida. Raw seawater samples were collected from the sites and delivered to the bench-scale testing facility at MWH in California and at the University of Illinois, Urbana-Champaign (UIUC). Water quality parameters such as pH, conductivity, and temperature were measured at the time of sampling. Upon receipt of the source water, samples were stored in a refrigerator at 4 °C to reduce microbial growth.

2.1.1 Basic Water Quality Analysis

Raw seawater samples were analyzed at MWH Laboratories in California. Methods used for analyzing basic water quality parameters along with the respective dilutions required due to the high salt matrix are listed in Table 2.1.

Carbohydrate Analysis

Raw seawater samples were mixed with potassium ferricyanide (0.7 mM) and kept for 10 min in a boiling-water bath to form an initial reagent mixture. One milliliter of ferric chloride (2 mM) and 2 mL of 2,4,6-tripyridyl-*s*-triazine were added to the mixture and mixed in a vortex mixer. Absorbance measurements at 595 nm were taken after 30 min for the samples mixed with various reagents. Standard absorbance curves with D-glucose were generated and compared with absorbance of the sample. Absorbance of Milli-Q water was used as a blank. For measuring polysaccharide content, 4 mL of seawater sample and 0.4 mL of 1 M HCl were added to 5-mL glass cuvettes. The samples were placed in a heat cabinet at 150 °C for 1 h. After hydrolysis was completed, the sample was cooled and neutralized with 1 M NaOH and weighed. The samples were then quantified using a standard curve. The concentration of polysaccharides was calculated by subtracting the monosaccharide content using the standard curve based on D-glucose (Myklestad et al., 1997).

Table 2.1. Analytical Methods Used for Seawater Characterization^a

Parameter	Method	Dilution
TDS	SM 2540-C	1
Turbidity	SM 2130B	1
TOC	UV-Persulfate	5
Protein	Lowry	5
Temperature	SM 2550B	1
pH	SM 4500H ⁺	1
Conductivity	SM 2510B	1
Calcium	EPA 200.7	20
Magnesium	EPA 200.7	20
Potassium	EPA 200.7	20
Sodium	EPA 200.7	50
Barium	EPA 200.8	10
Strontium	EPA 200.7	10
Bromide	EPA 300	500
Fluoride	SM 4500F-C	1
Nitrate	EPA 300.0	50
Chloride	EPA 300.0	1000
Sulfate	EPA 300.0	50
Silica	EPA 200.7	20
Boron	EPA 200.7	20
Fecal Coliform	SM 9221C	1
Total Coliform	SM 9221B	1

^aTDS, total dissolved solids.

2.1.2 Size Distribution of Organic Matter

High-performance size exclusion chromatography (HPSEC) was used to quantify the size distribution of organic matter present in seawater samples. A column with a molecular weight separation range of 2 to 80 kDa (Protein-Pak 125; Waters, Milford, MA) was calibrated with polystyrene sulfonate standards (Polysciences, Inc., Warrington, PA). The polystyrene sulfonate standards used were 1.8, 4.6, 8.0, 18.0, 35.0, and 67.0 kDa. Detection was by UV absorbance in the range of 200 to 300 nm, with a resolution of 1 nm.

2.2 MEMBRANE SELECTION AND CHARACTERIZATION

Three different SWRO thin-film composite membranes were used for the study. The model membranes used were SWC4 (Hydranautics, Oceanside, CA), SW30HR (Dow Filmtec, Midland, MI), and RE4040-SR (Saehan, Seoul, SouthKorea). Hydranautics SWC4 and DowFilmtec SW30HR were obtained as flat sheets from the manufacturer. Saehan RE4040-SR membranes were cut from a 4-in. spiral-wound element. Membranes were stored in deionized (DI) water at 4 °C with water replaced weekly.

2.2.1 Surface Potential

Membrane surface zeta potential was determined with a streaming potential analyzer. When membranes are immersed in water, they acquire a surface charge. Because of the presence of co-ions and counter-ions formed on the outer layer of the surface, a charged double layer comprised of counter-ions near the surface and co-ions farther away from the surface is created. Both the membrane surface and the foulant (organic/biological) when immersed in

water would form a double layer of charges on the surface. A compact layer and a diffuse double layer are present on the surface of the membrane. The compact layer (stern layer) is immobile, whereas the diffuse double layer is mobile. A plane of shear separates the immobile and mobile layers. An example of an electrical double layer is shown in Figure 2.1. The principle of operation is based on the streaming potential method in which an electrolyte solution is pumped through the measuring cell containing the membrane, creating a pressure difference. A relative movement of the electrical double layer formed over the membrane surface occurs and gives rise to streaming potential. A plane of shear is present between the charged stationary and mobile layers on the membrane surface. The zeta potential (ζ) is the potential present at the plane of shear (Childress and Elimelech, 1996). The streaming potential measured from the instrument is converted to the zeta potential of the membrane surface. Three runs on three separate days were performed for three different samples of each membrane at various ionic strengths and a range of pH values.

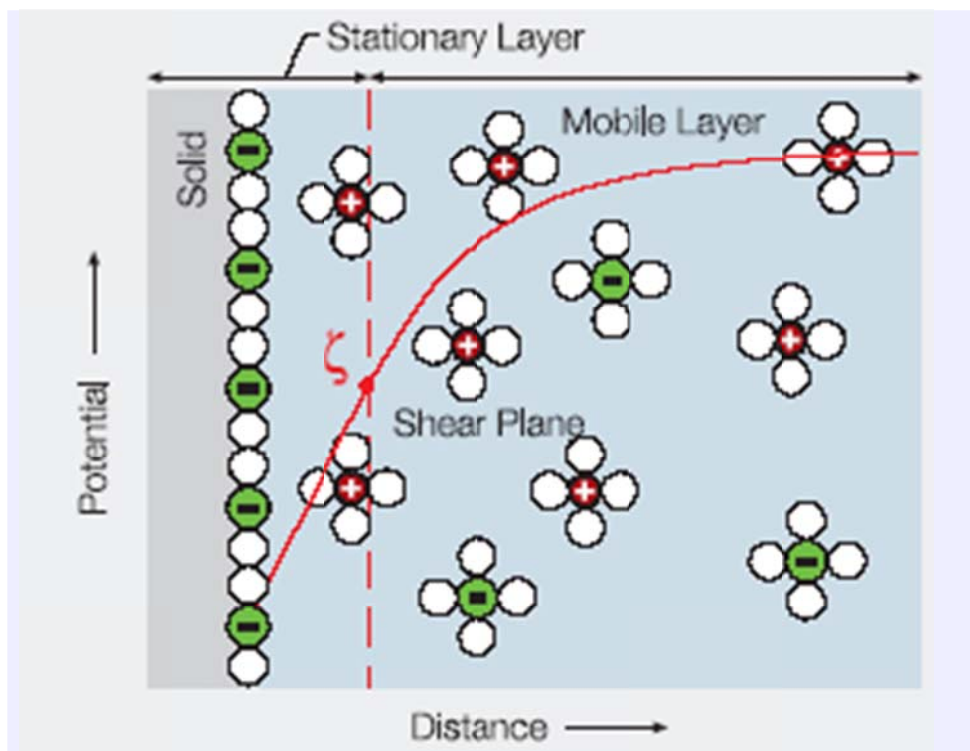


Figure 2.1. Electrical double layer formed at the membrane surface (www.antonparr.com).

2.2.2 Surface Roughness

Membrane surface roughness was determined by atomic force microscopy (AFM) imaging and analysis. AFM relies on measuring the force (van der Waals) between a special tip and the sample. The force is indirectly measured but can be calculated from the tip deflection and cantilever spring constant. Tapping mode AFM measurements were conducted using an etched silicon probe (Vrijenhoek et al., 2001). Clean membrane coupons were allowed to dry for 24 h in a desiccator before AFM scans were performed. For an analysis containing N data points, the RMS roughness is given by the standard deviation of the individual height measurements:

$$R_{rms} = \sqrt{\frac{\sum_{n=1}^n (z_n - \bar{z})^2}{N-1}} \quad (1)$$

Where \bar{z} is the mean z height, which is given by the average of the individual height measurements:

$$\bar{z} = \frac{1}{N} \sum_{n=1}^N z_n \quad (2)$$

2.2.3 Contact Angle Analysis

Contact angle measurements were obtained using a Kruss goniometer (Brant and Childress, 2002). The contact angle between the solid surface and a liquid droplet is used to measure the surface energy. Measurement of surface energy through contact angle analysis is strongly dependent on the surface chemistry of the solid (membrane). Clean membrane coupons removed from the DI water storage were dried in a desiccator for 24 h before collection of contact angle measurements. The membrane coupons were attached to a glass slide using double-sided tape. At least eight equilibrium contact angles were determined for each membrane with the highest and lowest values discarded. The average of left and right contact angles was taken as the equilibrium contact angle.

2.2.4 Surface Functionality

ATR-FTIR spectrometry was used to study the organic functionalities of both clean and fouled membranes (Kumar et al., 2006). The membrane sample was attached to a crystal, and IR radiation was passed through an internal reflection element (IRE). The IR radiation was reflected several times within the crystal and detected using a spectrometer. An illustration is shown in Figure 2.2. The depth of penetration of the IR beam into the membrane sample is $\sim 1 \mu\text{m}$. Absorption in the mid-IR region ($4000\text{--}600 \text{ cm}^{-1}$) can provide a means to acquire a unique spectroscopic fingerprint for each membrane and organic foulant. Small rectangular pieces of dry membrane (clean and fouled) were pressed against an IRE. The IRE sample holder was then placed on the ATR mirror assembly in the sample compartment of an FTIR spectrometer. Single-beam sample spectra were obtained by signal averaging multiple (256) scans at a resolution of 4 cm^{-1} . Each sample spectrum was ratioed against a bare IRE background spectrum and then converted to absorbance. Energy dispersive spectroscopy (EDS) was used to determine the inorganic composition of the foulant layer. In EDS, a beam of X-ray is focused on the sample. The number and energy of the emitted X-ray beam were detected by using an energy dispersive spectrometer. As the energy of the emitted X-rays is characteristic of the atomic structure of the element from which they were emitted, the detector allows the elemental composition of the specimen to be measured.

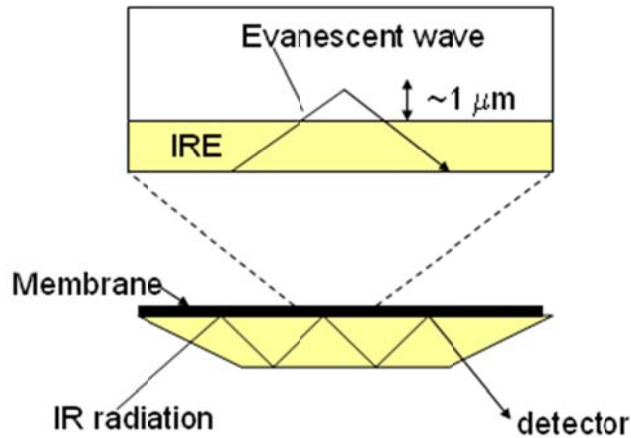


Figure 2.2. Illustration of ATR principle.

2.2.5 Surface Morphology

Qualitative surface morphology of the membranes was determined using scanning electron microscopy (SEM; Elimelech et al., 2006). SEM is a powerful technique for imaging microstructures on surfaces that has been applied to characterization of membranes and for studying membrane fouling. A stream of electrons is accelerated onto the membrane surface using an electron gun and a condenser lens. When the electron beam strikes the membrane sample, electrons are scattered back from the surface and observed using a detector. SEM relies on the scattering of electrons off the membrane surface to determine its surface structure. Before performance of SEM analysis, membrane samples were dried overnight in a desiccator. After drying, membrane samples were sputter coated using Ag/Pd for 60 s prior to SEM analysis. Images at various magnifications were obtained to qualitatively view the surface morphology of the model membranes.

2.3 FOULANT CHARACTERIZATION

Foulant was characterized for morphology and inorganic elemental analysis by SEM and EDS, respectively. Organic constituents of the foulant layer were analyzed by ATR-FTIR spectroscopy. The hydrophobicity of the foulant layer was analyzed using contact angle measurements. Individual methods are described in detail in the previous section. An illustration of techniques used to characterize a fouled membrane appears in Figure 2.3. The presence of biofilms on the membrane surface can also be determined using SEM. The EDS analysis was also used to determine if any corrosion-related products were deposited on the membrane surface. Quantification of change in surface roughness of the membrane was analyzed using tapping mode AFM measurements. Equilibrium contact angle analysis was performed using three liquids to determine the change in surface hydrophobicity of the membrane due to foulant deposition.

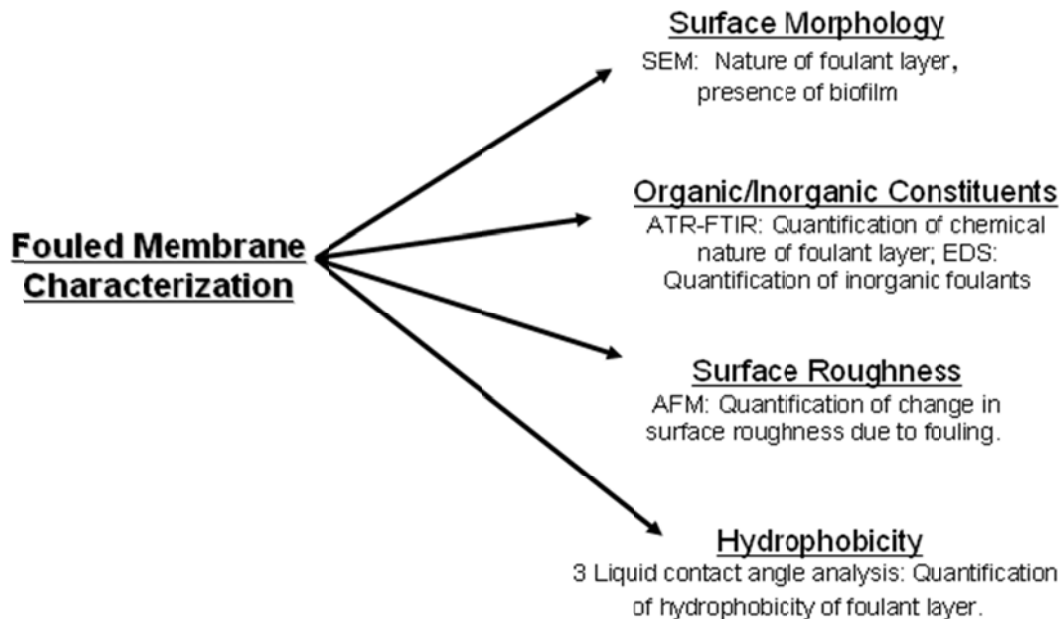


Figure 2.3. Illustration of foulant characterization techniques.

2.4 BENCH-SCALE TESTING

Membrane performance properties were evaluated at MWH using the bench-scale experimental setup shown schematically in Figure 2.4 and pictorially in Figure 2.5. The testing module is constructed of stainless steel and can accommodate a 155-cm² flat sheet membrane. Water was pumped to the test cell using a high pressure-pump to provide the appropriate operating pressure. Membrane coupons were cut from flat sheet rolls and allowed to soak in DI water for at least 24 h. Membranes were then loaded into the test cell and equilibrated before the fouling tests. Detailed description for bench-scale experiments is provided in the following chapter. A detailed protocol for conducting bench-scale experiments with seawater is provided in Appendix A.

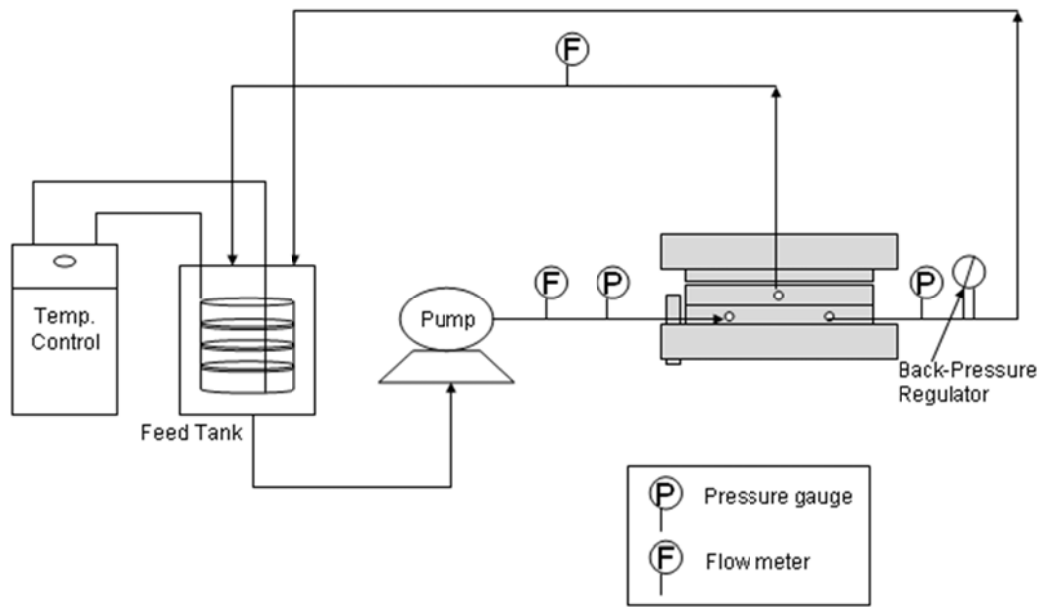


Figure 2.4. Schematic of bench-scale experimental setup.

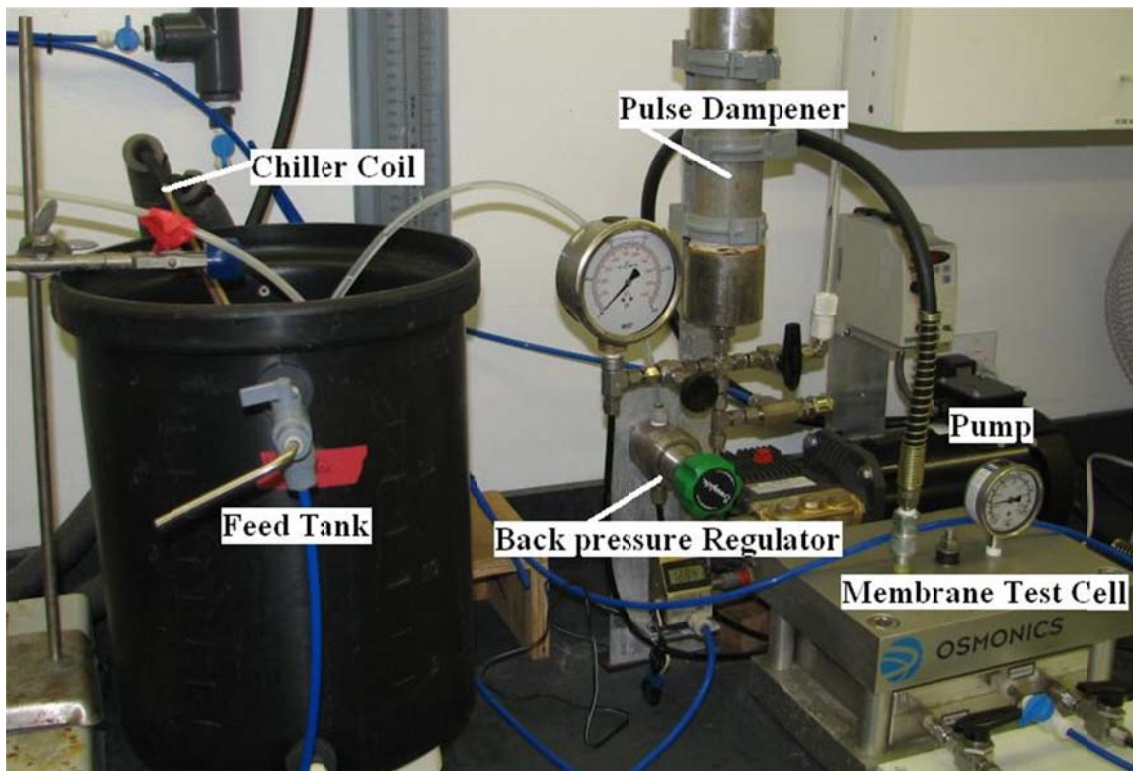


Figure 2.5. Picture of bench-scale experimental setup.

2.4.1 Equilibration Study

After the experimental setup was cleaned, equilibration and compaction experiments were carried out with a solution of sodium chloride at ~50 mS/cm (similar to seawater). A constant pressure of 1000 psi was used for the equilibration study. Equilibration was performed until no significant decrease in flux occurred with time. The equilibration run served to compact the membrane in preparation for fouling experiments and provided a baseline to compare different coupons.

2.4.2 Seawater Fouling Study

After the clean-water flux run, seawater was tested for fouling. Unless mentioned, all source seawaters were prefiltered through a 0.45- μm -pore-size cartridge filter. Because one of the objectives was to study organic fouling, prefiltration through a 0.45- μm -pore-size filter resulted in only the dissolved organic fraction of seawater to be utilized in the RO bench-scale system. The system was operated under constant pressure (1000 psi) for 24 h. The duration of the tests was determined from initial testing during this study where shorter (8 h) and longer (up to 5 days) runs were compared. From initial tests during this study, it was determined that 24 h was enough time for foulants to accumulate and observe a measurable flux decline in high fouling seawater sources. Shorter periods did not allow sufficient stabilization of flux and sufficient foulant accumulation. Performing bench-scale tests longer than 24 h also leads to corrosion issues in the system. Hence, experiments were planned to prevent rust buildup in the system components.

A constant crossflow velocity of 0.5 $\text{m}\cdot\text{s}^{-1}$ ($Re \sim 280$) was maintained throughout the experiments. Permeate and feed conductivity were measured periodically every hour. After the experimental run was complete, the system was cleaned by flushing with DI water for 30 min.

2.4.3 AOM Fouling Study

A marine bloom-forming dinoflagellate, *Heterocapsa pygmaea*, was used to study the influence of algogenic organic matter (AOM) fouling. *H. pygmaea* was grown in a sequencing batch culture. Growth of *H. pygmaea* was monitored using a fluorometer, and manual cell counts were determined with a hemacytometer. At exponential growth phase, the cells were extracted using centrifugation and added to seawater in the RO bench-scale system.

2.5 PILOT-SCALE ELEMENT AUTOPSY

An autopsy on the spiral-wound element obtained from Carlsbad was conducted at UIUC. The pilot plant was operated using Hydranautics SWC4+ membrane for a period of about 2 weeks at ~8-gfd flux. Membrane leaves from the lead element were shipped to UIUC for SEM, EDS, and ATR-FTIR analysis.

2.6 SURFACE ENERGY ANALYSIS

Contact angles obtained from three liquids were used to determine the surface energy parameters of the SWRO membranes and foulant. According to van Oss (1993), the surface tension (γ^{TOT}) of any medium can be divided into Lifshitz–van der Waals (γ^{LW}) and acid–base components (γ^{AB}). Thus, the surface tension is

$$\gamma^{TOT} = \gamma^{LW} + \gamma^{AB} \quad (3)$$

with

$$\gamma^{AB} = 2\left(\sqrt{\gamma^+ \gamma^-}\right) \quad (4)$$

In this equation γ^+ and γ^- are the electron-acceptor and electron-donor parameters of the acid–base component of the surface tension, respectively. Individual surface tension components γ^{LW} , γ^+ , and γ^- were determined using contact angle measurements with at least three different liquids with well-known surface tensions (Brant and Childress, 2002). Surface tension components were determined from the extended Young equation (van Oss, 1993):

$$(1 + \cos \theta)\gamma_l^{TOT} = 2\left(\sqrt{\gamma_s^{LW} \gamma_l^{LW}} + \sqrt{\gamma_s^+ \gamma_l^-} + \sqrt{\gamma_s^- \gamma_l^+}\right) \quad (5)$$

In this equation, θ is the contact angle, γ^{TOT} is the total surface tension, γ^{LW} is the Lifshitz–van der Waals component, and γ^+ and γ^- are the electron-acceptor and electron-donor components, respectively.

The subscripts s and l represent the solid surface and the liquid, respectively. The surface tension components can be used to evaluate the free energy components per unit area, $\Delta G_{h_0}^{LW}$ and $\Delta G_{h_0}^{AB}$, as follows (Brant and Childress, 2002):

$$\Delta G_{h_0}^{LW} = 2\left(\sqrt{\gamma_l^{LW}} - \sqrt{\gamma_m^{LW}}\right)\left(\sqrt{\gamma_c^{LW}} - \sqrt{\gamma_l^{LW}}\right) \quad (6)$$

and

$$\Delta G_{h_0}^{AB} = 2\sqrt{\gamma_l^+}\left(\sqrt{\gamma_m^-} + \sqrt{\gamma_c^-} - \sqrt{\gamma_l^-}\right) + 2\sqrt{\gamma_l^-}\left(\sqrt{\gamma_m^+} + \sqrt{\gamma_c^+} - \sqrt{\gamma_l^+}\right) - 2\sqrt{\gamma_m^+ \gamma_c^-} - 2\sqrt{\gamma_m^- \gamma_c^+} \quad (7)$$

In these equations the subscripts m , c , and l represent membrane, colloid, and liquid, respectively, and h_0 is the minimum equilibrium cutoff distance of 0.158 nm (van Oss, 1993).

Chapter 3

Results and Discussion

3.1 FEED WATER CHARACTERISTICS

Basic feed water characteristics for all the seawater sources were quantified, and average values are listed in Table 3.1. Water samples were collected during the period of July–August 2007 for WBMWD, TBDP, and CDP, whereas for SBPP they were collected during April 2007. The (SDI)₁₅ values were higher for TBDP and SBPP raw seawater than for CDP and WBMWD raw seawater. Thus, substantial pretreatment of the TBDP and SBPP seawater might be essential in order to decrease RO fouling due to particulates. Among the individual ionic species present, chloride and sodium were found to be the dominant ions in all the seawater sources. Among the divalent ions, magnesium was found to be present in higher concentrations than calcium. The concentration of magnesium and calcium was higher for WBMWD and SBPP than for the other two seawater sources. When polysaccharides are present in seawater, calcium ions bind with the carboxylic functionality present in polysaccharide molecules and form Ca²⁺-polysaccharide aggregates. The formation of such aggregates leads to significant flux decline due to formation of a gel-like layer on the membrane surface during RO plant operation (Li et al., 2007). Concentration of boron was > 4.0 mg/L for WBMWD and SBPP. Boron concentrations were lower for TBDP and CDP seawaters. Because boron is uncharged in the natural seawater pH range, rejection by RO membranes is low without pH adjustment.

Total silica concentrations in all the seawaters sources were low (<7.0 mg/L). Because silica concentrations were low, reactive and colloidal components of silica were not analyzed. The presence of silica in colloidal form can lead to colloidal fouling of RO membranes, and the presence of reactive silica can lead to precipitative fouling. Metals such as iron, copper, nickel, and aluminum were not detected in the raw seawater source. The temperature of seawater can play an important role in microorganism growth and hence biofouling potential of seawater (Al-Ahmad, 2000). Because the seawater was collected and shipped to the labs in California and Illinois, changes in temperature would have occurred. Hence, influence of raw seawater temperature is not reported in this study.

Table 3.1. Chemistry of Various Seawater Sources^a

Analyte	Units	Location			
		West Basin	Tampa Bay	Carlsbad	South Bay
Alkalinity in CaCO ₃ units	mg/L	114	155	92	110
Bicarb. alkalinity as HCO ₃	mg/L	140	190	110	130
pH	pH units	8	7.8	7.9	7.8
(SDI) ₁₅	—	4.3	6.3	4	5.8
TDS	mg/L	33,660	31,150	33,040	33,450
TOC	mg/L	< 1	2.5	< 1	NA
Boron	mg/L	4.7	3.8	2.4	4.6
Barium	µg/L	ND	ND	ND	ND
Bromide	mg/L	62.6	56.2	66.4	60.6
Strontium	mg/L	7.3	6.6	7.4	7.3
Calcium	mg/L	390	360	200	400
Magnesium	mg/L	1300	1100	650	1300
Potassium	mg/L	380	320	190	370
Sodium	mg/L	11,000	8800	5200	10,000
Chloride	mg/L	19,000	16,000	19,000	18,000
Fluoride	mg/L	1	0.9	0.9	0.9
Sulfate	mg/L	2700	2000	3000	2660
Silica	mg/L	ND	6.7	3.5	NA
Iron	mg/L	ND	ND	ND	NA
Copper	mg/L	ND	ND	ND	NA
Nickel	mg/L	ND	ND	ND	NA
Aluminum	mg/L	ND	ND	ND	NA
Ammonia nitrogen	mg/L	ND	0.1	0.1	0.08
Chlorophyll <i>a</i>	mg/L	<2.0	<2.0	<2.0	NA
Fecal coliform bacteria	MPNM	<2.0	<2.0	17	2
Total coliform bacteria	MPNM	<2.0	<2.0	17	8

^aND, not detectable; NA, not available ; TDS, total dissolved solids.

In order to quantify algal presence in the seawater source, chlorophyll *a* concentrations were determined using UV absorption. Chlorophyll *a* was not detected in any seawater source. Because chlorophyll *b* and chlorophyll *c* are in general at a lower concentration than chlorophyll *a*, they were not analyzed (Leparc et al., 2007). Higher chlorophyll *a* concentrations are possible in the seawater when an algal bloom (red tide event) occurs. All seawater sources collected during this study did not have the influence of algal blooms. Although in this study the water samples tested were not under the influence of algal blooms, when an algal bloom occurs, more than 25% of pigment concentrations have been reported to pass through conventional pretreatment processes (Leparc et al., 2007). Hence, during algal blooms, a substantial amount of pigment concentration can pass through conventional prefiltration and reach the SWRO membrane. TOC concentrations were measured to determine the total organic content in the various seawater sources. In order to measure TOC, samples were diluted five times to reduce interference due to high chloride concentrations. Because of dilution of the samples, TOC concentrations for most sources tested were below the lowest detection limit (0.5 mg/L) except for TBDP. Seawater from TBDP had a TOC concentration of 2.5 ± 0.7 mg/L.

In seawater, the presence of polysaccharides and transparent exopolymers exuded by phytoplankton and bacteria can lead to the transformation of dissolved organic matter into particulate form. Polysaccharides produced from phytoplankton and bacteria in seawater were

reported to be present in high abundance (Allredge et al., 1993). Carbohydrate compositions (as milligrams per liter of glucose) for all the source waters are shown in Figure 3.1. Two measurements were performed for hydrolyzed and nonhydrolyzed samples. Hydrolyzed samples were heated at 100°C overnight with hydrochloric acid to convert polymeric carbohydrates to their monomeric subunits. Because the assay is sensitive only to monomeric sugars, the difference between the hydrolyzed and the nonhydrolyzed samples is the polysaccharide concentration. All the seawater sources have polysaccharides present, with TBDP water having the highest monomeric and polymeric fraction of the carbohydrate content. To determine the size fraction of the polysaccharides, HPSEC analysis was performed. Although peaks were found of <1.8 kDa, the lowest concentration of standards used was 1.8 kDa, and hence the values obtained for the seawater sources were below the standard concentration and irreproducible. Protein concentrations in the seawater sources are also not reported because of dilution of samples leading to quantification below detection limits.

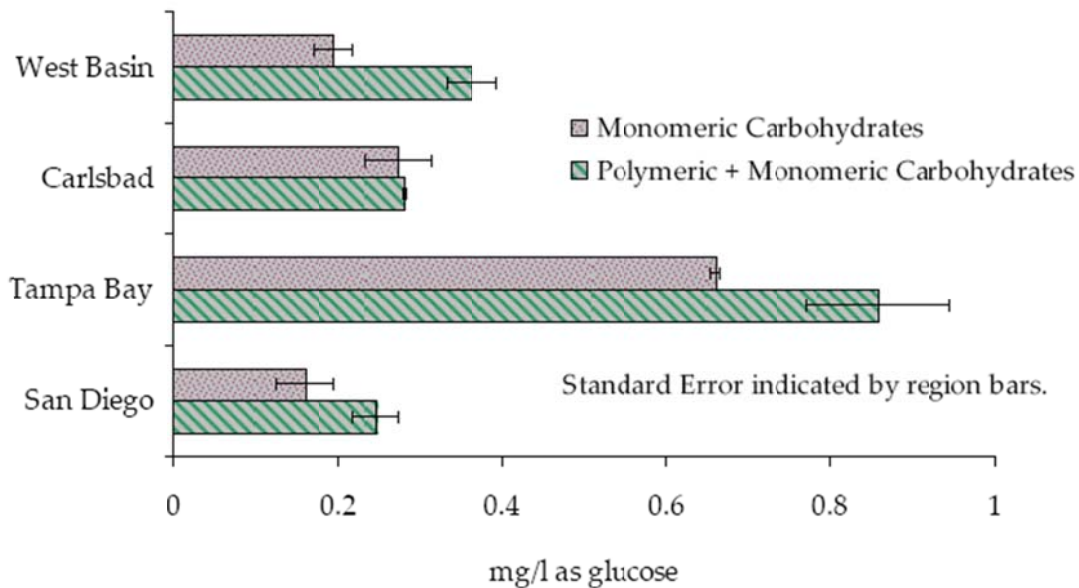


Figure 3.1. Measured carbohydrate concentrations for the various seawater sources.

3.2 CLEAN MEMBRANE CHARACTERISTICS

SWRO membranes are primarily of thin-film composite polyamide (TFC-PA) composition. Based on the manufacturing procedure and surface modifications used during the manufacturing process, membrane surface properties such as surface charge, roughness, and hydrophobicity vary. Hence, an array of characterization techniques was utilized to determine the membrane surface properties.

3.2.1 Surface Morphology using SEM

In order to qualitatively determine the surface morphology of clean membranes, SEM was performed on the model membranes. SEM images of clean SWRO membranes are shown in

Figure 3.2. The SEM images shown were obtained at a magnification of 10,000 \times . All three SWRO membranes have a rough surface morphology that is typical for TFC-PA membranes. SEM images of Saehan SR membrane at higher magnifications (50,000 \times and 75,000 \times) are shown in Figure 3.3. The images show a complex morphology of the polymer matrix found on the membrane surface.

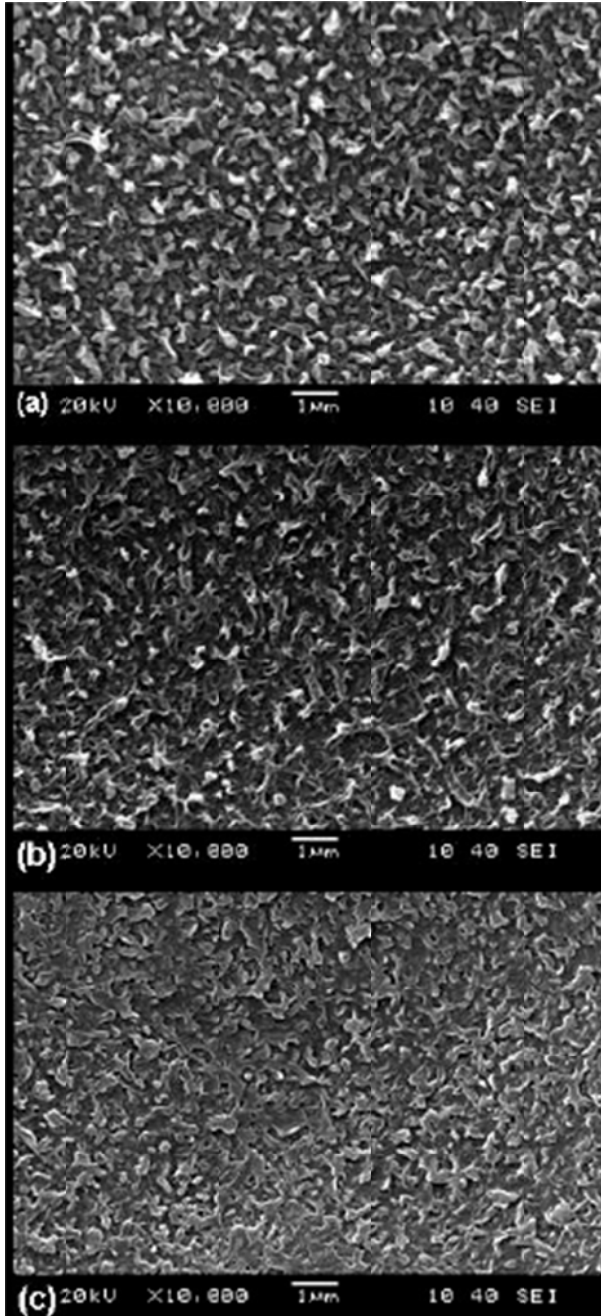


Figure 3.2. SEM images of clean (a) Hydranautics SWC4, (b) Saehan SR, and (c) DowFilmtec SW30HR membranes.

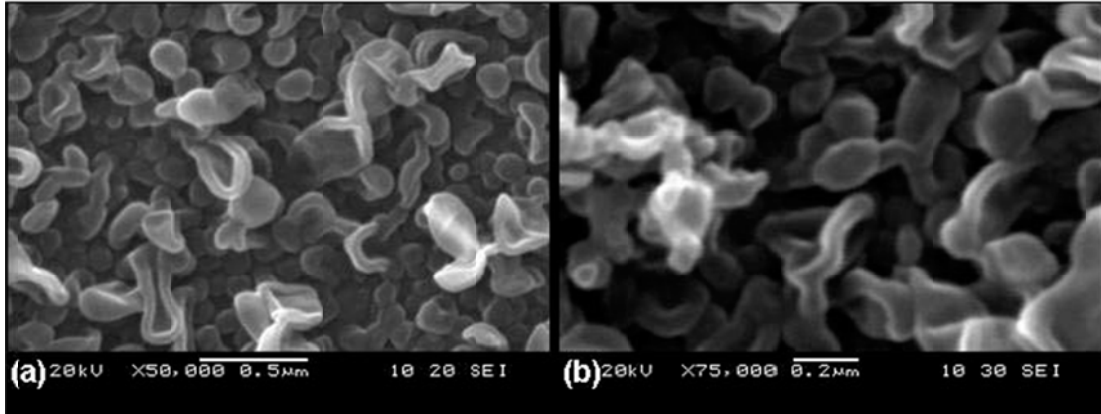


Figure 3.3. SEM images of the Saehan SR membrane at (a) 50,000× and (b) 75,000× magnifications.

3.2.2 Surface Charge using Streaming Potential Measurements

The distribution of charged ions near a membrane surface is dependent on the solution chemistry (pH and ionic strength) because they influence protonation/deprotonation of the membrane surface functionality. In the case of low-ionic-strength solutions, the electrical potential decreases steadily until it reaches a distance where electroneutrality exists. For seawater, because of very high ionic strength, electrostatic double layer interactions between the membrane and the foulant can be significantly suppressed and the potential decreases steeply near the membrane surface.

Zeta potentials calculated from streaming potential measurements obtained for the model membranes are shown in Figure 3.4. The streaming potential of Hydranautics SWC4 membrane was tested over a wide pH range and under different ionic strengths (1 mM, 10 mM, and 100 mM). Because of deprotonation of the carboxylate functional groups on the polyamide membrane surface, the zeta potential decreases (becomes more negative) with an increase in pH (Childress and Elimelech, 1996). The zeta potential increases (becomes less negative) with an increase in ionic strength. Because of double layer compression, the values of the zeta potential in the range of operational pH values for SWRO operations tend to become less negative, indicating a higher fouling potential of negatively charged organic material at higher salinity conditions.

Streaming potential was also measured at a pH of 8.0 for the other two model membranes (DowFilmtec SW30HR and Saehan SR) at an ionic strength of 100 mM. Under these high-ionic-strength conditions, their zeta potential values are quite similar. A similar zeta potential value indicates that the electrostatic repulsive force between the membrane and foulant material will be similar. At high ionic strengths (> 100 mM), the instrument is incapable of determining streaming potential measurements.

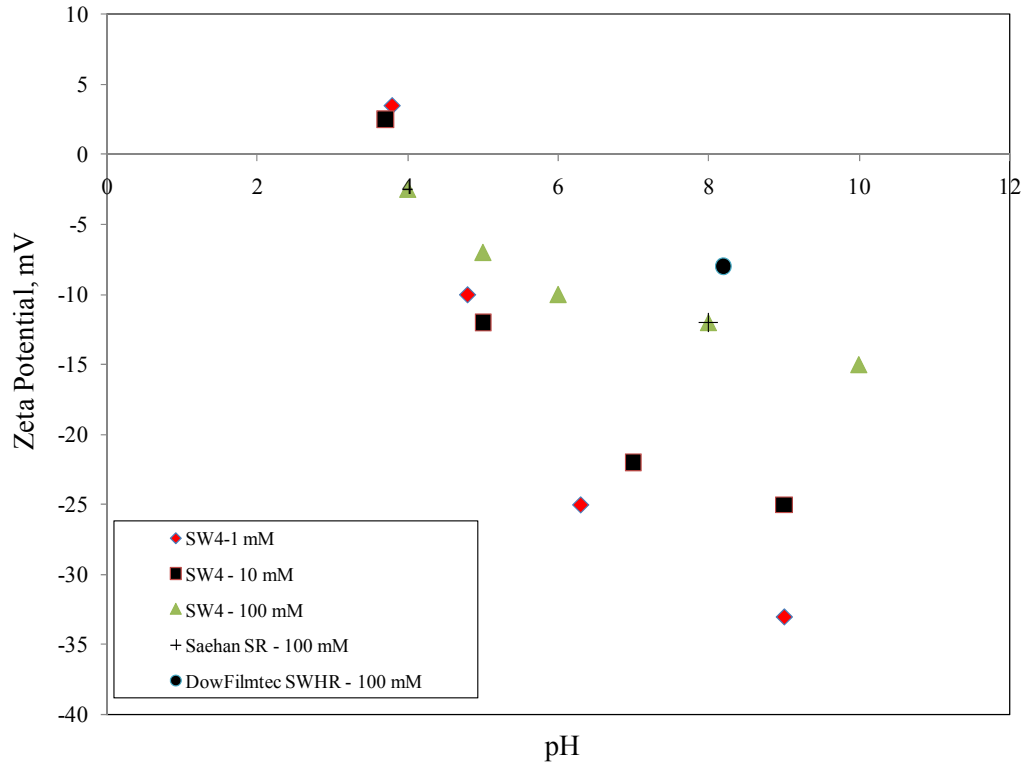


Figure 3.4. Zeta potential as a function of pH and ionic strength for the model membranes.

3.2.3 Surface Roughness using AFM

Surface roughness of the model membranes was determined using AFM. AFM topographs were obtained for all three membranes. The 2D and 3D images obtained from these measurements are shown in Figure 3.5. From the AFM images and the roughness values, it appears that the DowFilmtec SW30HR and Saehan SR membranes have similar surface topologies, whereas the Hydranautics SWC4 has significantly higher roughness. The measured roughness parameters for the model SWRO membranes used in this study are shown in Table 3.2. Root mean square (RMS) roughness and average roughness ($R_{average}$) are reported. The Hydranautics SWC4 membrane has significantly higher roughness than do the DowFilmtec SW30HR and Saehan SR membranes. Surface roughness of membranes can significantly reduce the range and magnitude of interfacial interactions (especially electrostatic interactions), leading to higher fouling potential (Hoek et al., 2003). Because of the presence of high ionic strength in seawater, the electrostatic interactions are further suppressed. Thus, rougher membranes (Hydranautics SWC4) will exhibit higher fouling potential than will relatively smoother membranes (DowFilmtec SW30HR and Saehan SR).

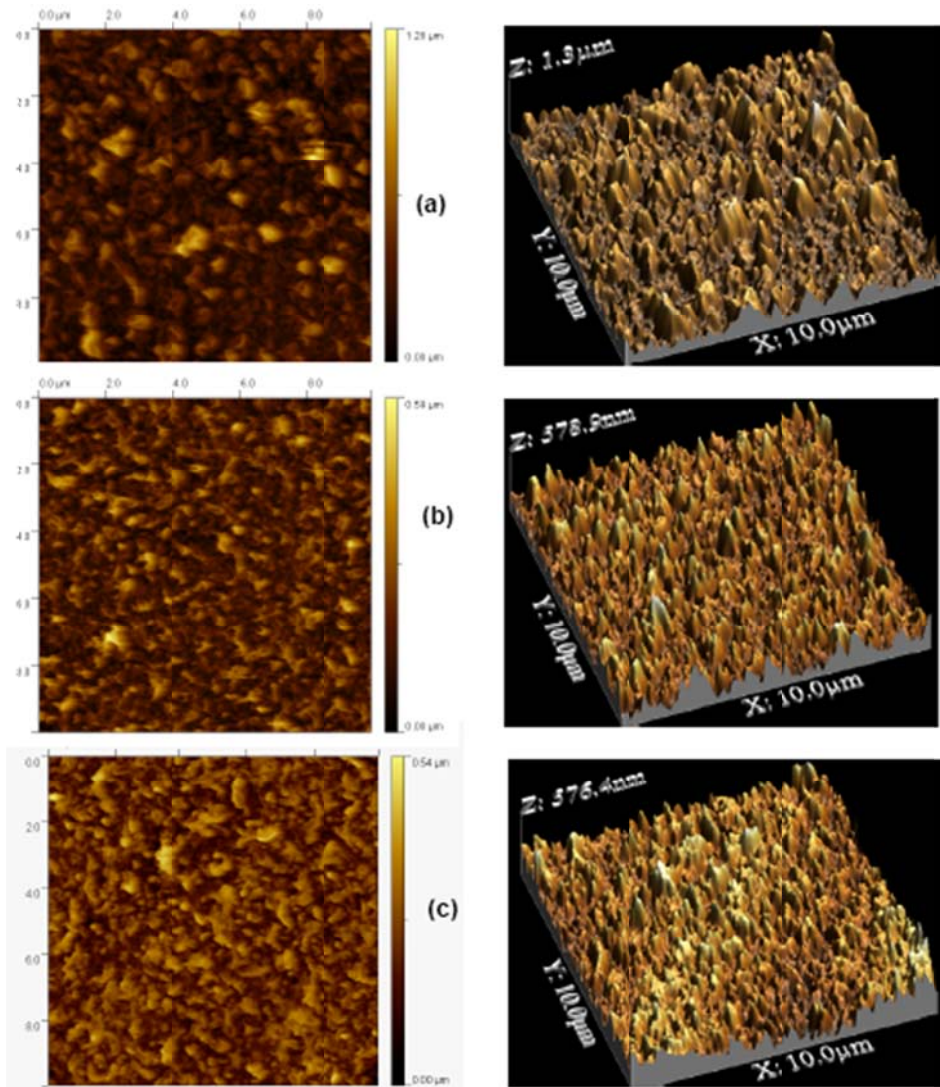


Figure 3.5. AFM topographs for different commercial dried virgin membranes: (a) Hydranautics SWC4, (b) Saehan SR, and (c) Dow SW30HR.

Table 3.2. Roughness Parameters for Clean Membranes

Membrane	RMS Roughness	Avg. Roughness	No. of Samples
Hydranautics SWC4	150.5 ± 5.4	117.9 ± 3.4	3
DowFilmtec SW30HR	78.3 ± 7.8	62.3 ± 5.7	3
Saehan SR	79.1 ± 3.0	63.1 ± 3.2	4

3.2.4 Surface Hydrophobicity using Contact Angle Measurements

In order to quantify the relative hydrophobicity of the three SWRO membranes, contact angle measurements using a goniometer were performed. It is important to determine the relative hydrophobicity for the model membranes due to the presence of acid–base interactions. Acid–base interactions are medium-based (water) interactions like van der Waals and electrostatic interactions. Acid–base interactions arise from hydrogen bonding. When the surface is hydrophobic, water experiences a repulsive force that disturbs the natural water structuring. When hydrophobic surfaces come in close contact with each other, water tries to migrate away from the two surfaces, leading to an attraction between the two hydrophobic surfaces. This is called an attractive hydrophobic interaction. The opposite effect occurs when two surfaces are hydrophilic in nature. These types of water-mediated interactions are called acid–base interactions (Grasso et al., 2002).

It is expected that membranes with relatively higher hydrophobicity will exhibit higher fouling potential. Images of DI water droplets on clean seawater membranes are shown in Figure 3.6. The DowFilmtec SW30HR membrane forms the smallest contact angle when compared to Hydranautics SWC4 and Saehan SR membranes.

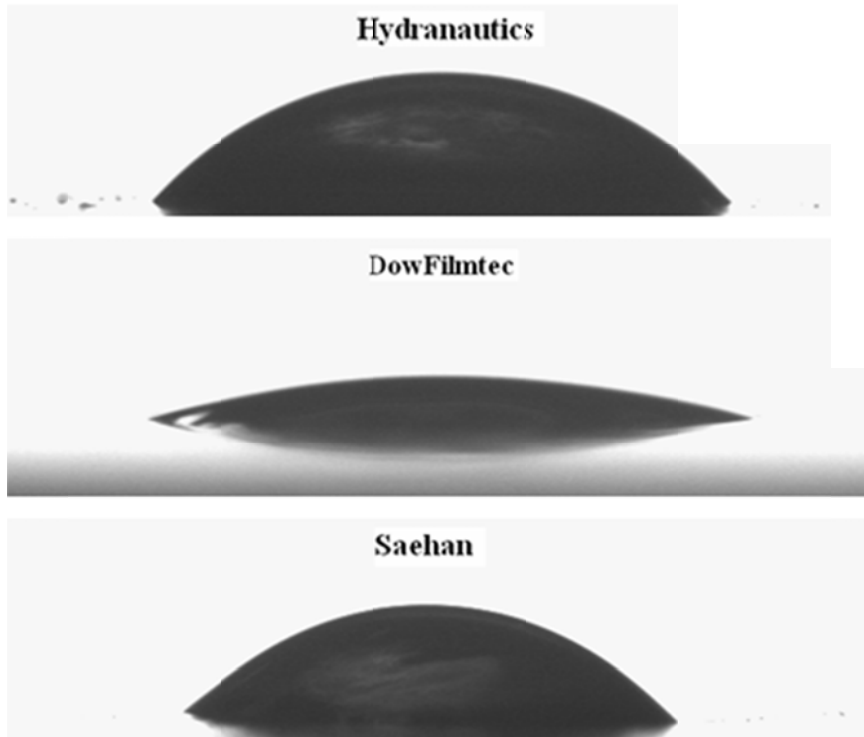


Figure 3.6. Images of DI water droplets on model membranes.

Because of the high ionic strength of seawater and the presence of various multivalent ions, contact angle measurements in seawater could differ from those determined with DI water. To evaluate this possibility, contact angle measurements were performed on a Hydranautics SWC4 membrane with both DI water and seawater obtained from West Basin. The contact angles obtained with seawater (54.8 ± 0.08) were different from the contact angle obtained with DI water (47.2 ± 4.02).

Because DI water does not accurately represent the contact angles for all media, the extent of hydrophobicity for the SWRO membranes was determined using the acid–base approach proposed using two polar (water, ethylene glycol) and one apolar (diiodomethane) medium (van Oss, 1993). The contact angles obtained using the three liquids on all the membranes are shown in Figure 3.7. The DowFilmtec SW30HR membrane had the smallest contact angle for polar liquids (water and ethylene glycol) when compared to the Hydranautics SWC4 and Saehan SR membranes. The DowFilmtec SW30HR membrane also had the greatest contact angle with the apolar (diiodomethane) liquid when compared to the other two membranes.

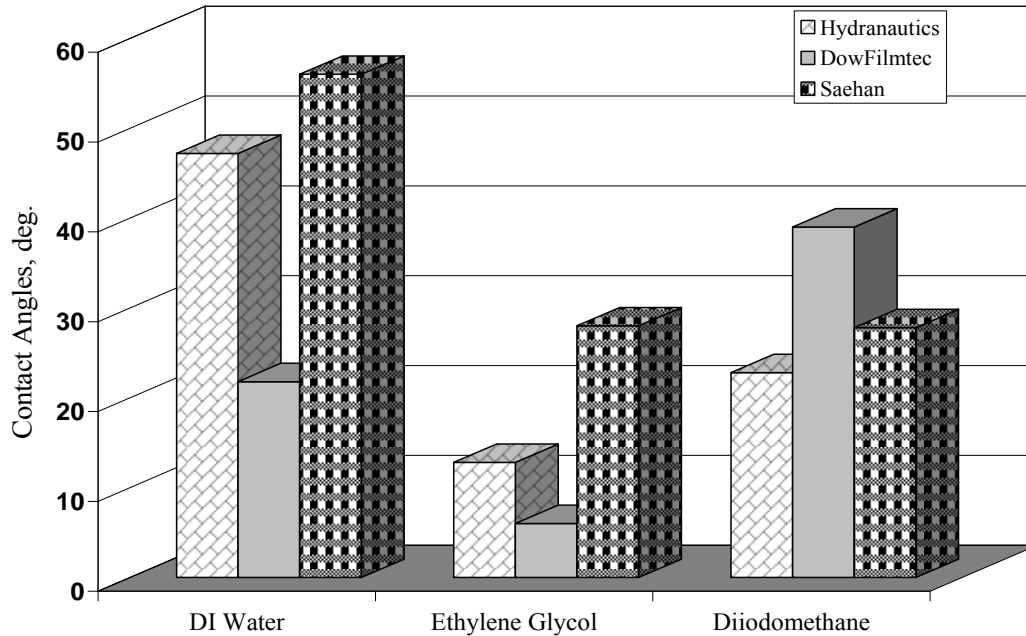


Figure 3.7. Comparison of contact angles using 3 liquids on model SWRO membranes.

Contact angles obtained from the three liquids were used to determine the surface energy parameters of the SWRO membranes. Calculated surface energy parameters for the model membranes are listed in Table 3.3. The Lifshitz–van der Waals component is lowest for DowFilmtec SW30HR membrane. Because of the small contact angles of the DowFilmtec SW30HR membrane with polar liquids, the electron-donor component for this membrane is significantly higher than for the other membranes. The presence of high electron-donor (γ^-) component on the membrane surface suggests the presence of more electron-donor surface functional groups exposed on the surface that could accept a proton from water to form structured layers of water molecules on the membrane surface, hence having a surface that is relatively hydrophilic. The free energy of cohesion (ΔG^{CO}) is the interaction free energy (per unit area) when two surfaces of the same material are immersed in solvent (water) and brought into contact. The free energy of cohesion was calculated using equations 6 and 7 and utilizing the properties of membrane and water alone. The free energy of cohesion values gives more quantitative insight into the hydrophobicity/hydrophilicity of the membranes. Positive values of the free energy of cohesion represent a hydrophilic surface, whereas negative values suggest a hydrophobic surface. Hence, the DowFilmtec SW30HR membrane

is more hydrophilic (positive ΔG^{CO}) than are the Hydranautics SWC4 and Saehan SR membranes (negative ΔG^{CO}).

Table 3.3. Surface Energy Parameters (mJ/m²) for Clean SWRO Membranes

Membrane	Values for:			
	γ^{LW}	γ^+	γ^-	ΔG^{CO}
Hydranautics SWC4	46.7	4.4	13.4	-25.8
DowFilmtec SW30HR	39.9	3.8	37.0	7.4
Saehan SR	44.9	3.9	9.3	-32.9

3.3 BENCH-SCALE TESTING OF DIFFERENT SEAWATER SOURCES

Fouling experiments were conducted with actual seawater immediately after compaction. Temperature-corrected normalized specific flux obtained from three seawater sources for studies conducted at both UIUC and MWH is shown in Figure 3.8a and Figure 3.8b, respectively. For all three seawater sources tested, the normalized specific flux did not vary significantly for the study conducted at UIUC and MWH. Similar trends were observed in both studies. Hence, the seawater samples collected for testing during this study did not exhibit a substantial decrease in normalized specific flux with time. Bench-scale tests were performed for only 24 h based on experience from previous studies where shorter (8 h) and longer (up to 5 days) runs were compared. From previous studies, it was determined that 24 h was enough time for foulants to accumulate and to observe measurable flux decline in waters. Shorter periods did not allow sufficient stabilization of flux. The normalized specific flux was lower for the studies conducted at MWH than in the data from UIUC. The normalized specific flux also dropped steeply after 16 h for the study conducted with West Basin seawater at MWH. After 16 h of operation, the salt passage also increased. The decreased flux obtained for MWH runs occurred because of corrosion issues encountered in the experimental setup and not because of changes in source-water chemistry. The issue of corrosion is described in detail later in the report. Because of corrosion debris being deposited on the membrane surface, observed rejection for studies conducted at MWH was about 1% lower than the rejection at UIUC. Conductivity rejection was about 98% (± 0.08) for the Hydranautics SWC4 membrane for the study conducted at MWH and was more than 99.3% (± 0.04) for the study conducted at UIUC. Although a difference in specific flux was not observed for the three seawater sources, deposition of foulant on the membrane surface is possible.

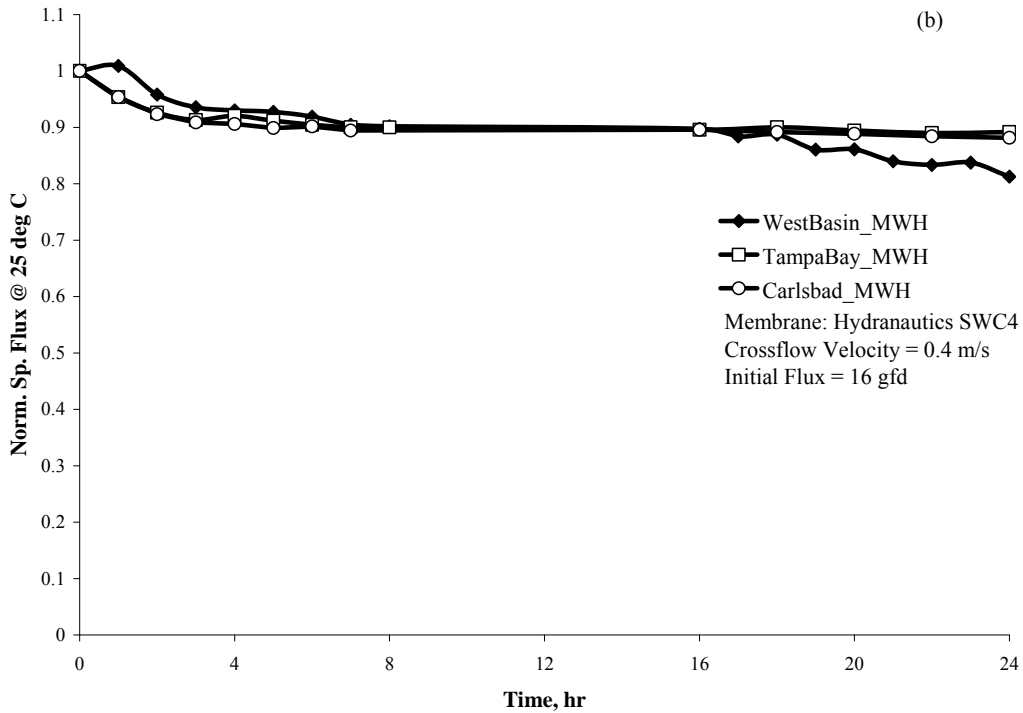
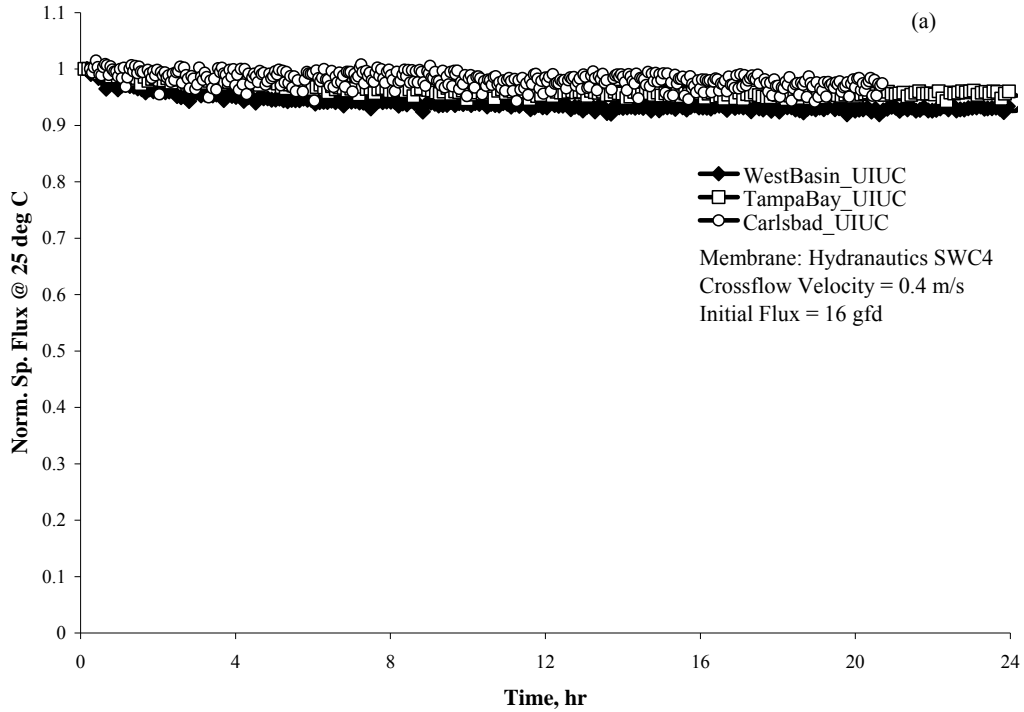


Figure 3.8. Normalized specific flux for all 3 seawater sources for studies conducted with Hydranautics SWC4 membranes performed at (a) UIUC and (b) MWH.

In order to determine if any foulant was deposited on the membrane surface, surface characterization techniques were performed on the membrane after the completion of the bench-scale study. Although there was no significant difference in the normalized specific flux for the three different seawater sources tested, foulants deposited on the membrane surface within the 24-h duration of the bench-scale study. SEM and AFM were used to characterize membrane foulants for bench-scale testing on seawater from three locations—West Basin, Tampa Bay, and Carlsbad. All samples were analyzed using SEM at three magnifications (600×, 3000×, and 10,000×). EDS analyses were also conducted to determine the presence of inorganic foulants on the membrane. AFM images were taken on a 10- μm \times 10- μm area for each sample. In the following paragraphs only images relevant to the discussion are provided.

3.3.1 Foulant Analysis of West Basin Seawater

The SEM image of the Hydranautics SWC4 membrane (UIUC sample) fouled with West Basin seawater is shown in Figure 3.9. Regions with film-like structures, granular structures and the membrane are clearly seen. EDS analysis performed on the film layer and granular structure is shown in Figure 3.10. EDS analysis of the film region shows the presence of iron. The granular region does not have iron.

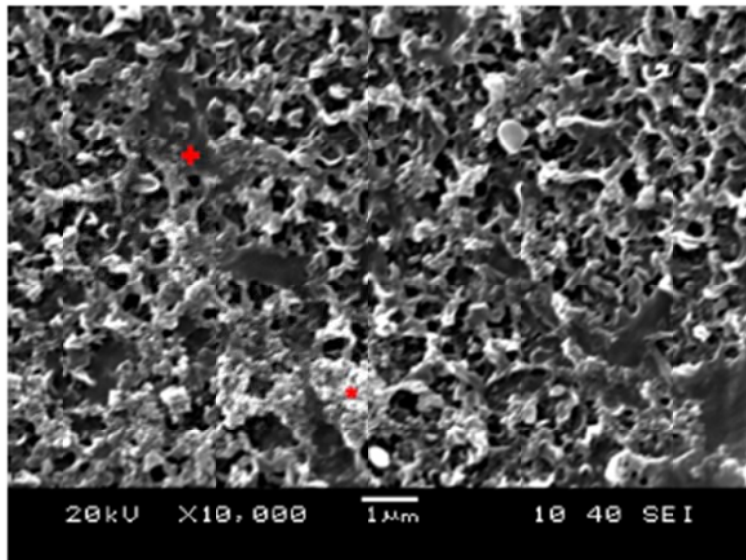


Figure 3.9. SEM image of Hydranautics SWC4 membrane fouled by West Basin seawater.

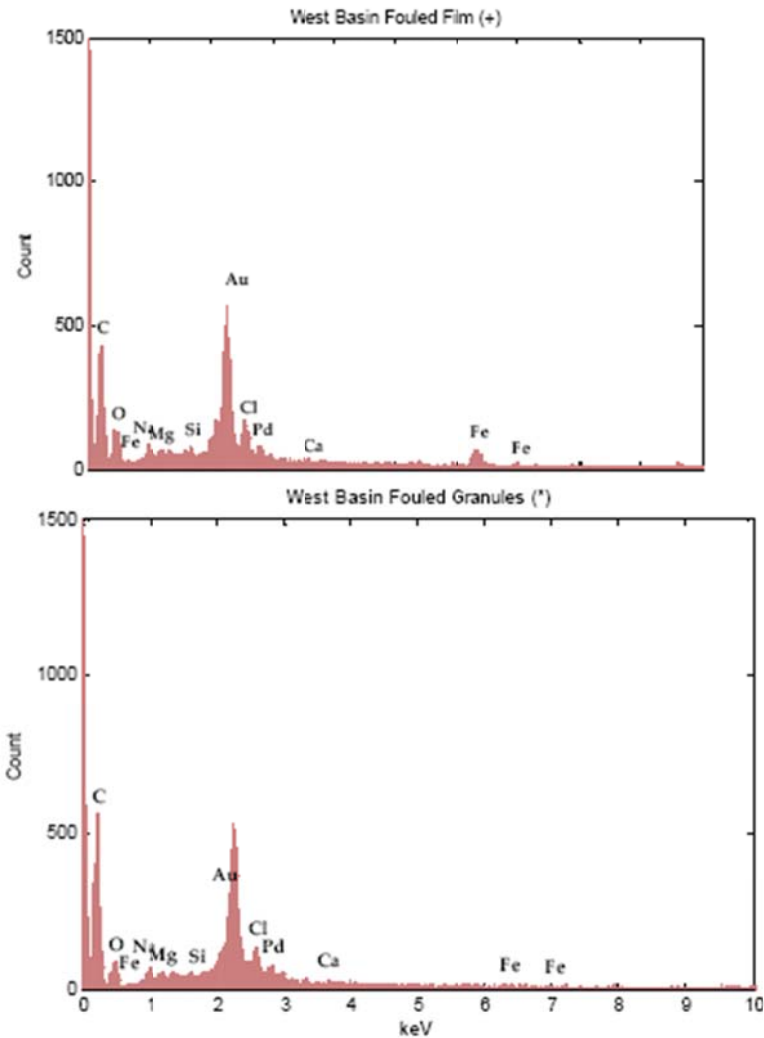


Figure 3.10. EDS analysis of Hydranautics SWC4 membrane fouled with West Basin seawater.

Deposition of foulants (organic/biological) on the membrane surface could lead to a significant change in the surface morphology (charge, hydrophobicity, and roughness) of the membrane surface, thus altering fouling behavior (Xu et al., 2006). Thus, AFM analysis was performed to determine if the surface morphology of the membrane changed after bench-scale fouling experiments. An AFM image of Hydranautics SWC4 membrane (UIUC sample) fouled with West Basin seawater is shown in Figure 3.11. The AFM image shows features similar to the SEM images. Roughness parameters for this membrane are also shown. The RMS roughness increased 30 nm compared to the clean membrane surface, but because of the presence of large heterogeneities, a rigorous analysis of the surface morphology using AFM was difficult to obtain. Moreover, AFM imaging over large areas is challenging, particularly with fouled membranes from which dirt can easily be transferred on to the AFM tip. Clean membrane surface properties influence fouling only for a certain period. Once a complete film or multilayer of foulants is deposited on the membrane surface, the physicochemical properties of the foulant play an important role in dominating deposition behavior. Thus, it is important to determine the change in surface properties of the membrane after fouling.

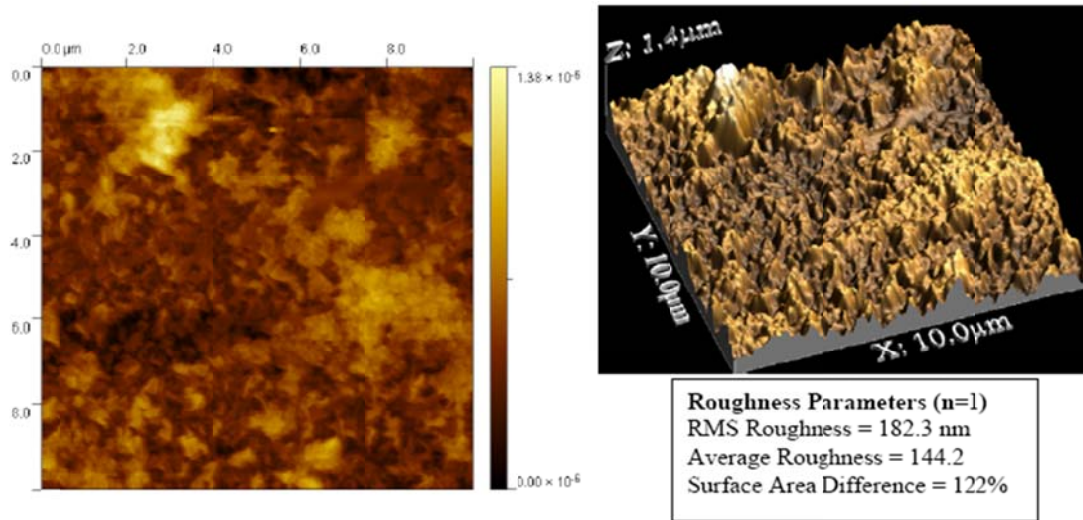


Figure 3.11. AFM topograph of Hydranautics SWC4 membrane fouled with West Basin seawater and roughness parameters.

Figure 3.12 shows the ATR-FTIR spectra for Hydranautics SWC4 membrane fouled with West Basin seawater. Five measurements were taken in the fouled portion of the membrane, and five measurements were taken from the unfouled edge of the coupon. Red indicates regions where the fouled-membrane spectrum rises above the edge spectrum, blue indicates where the edge spectrum rises above the fouled, and grey is the overlap. Thus, the red region represents the additional absorbance from the foulant layer in comparison to the clean membrane absorbance represented as the grey region. A small amount of material was detected in the foulant layer in the regions of 890 to 1050, 1620 to 1680, and 3000 to 3600 cm^{-1} . These regions are consistent with polysaccharide-like material (Jarusutthirak and Amy, 2002). Protein-like material was not prominent because a sharp peak at 3300 cm^{-1} and dual peaks at 1540 and 1640 cm^{-1} were absent (Jarusutthirak and Amy, 2002). Thus, polysaccharide-like material is more prominent than protein-like on the foulant layer.

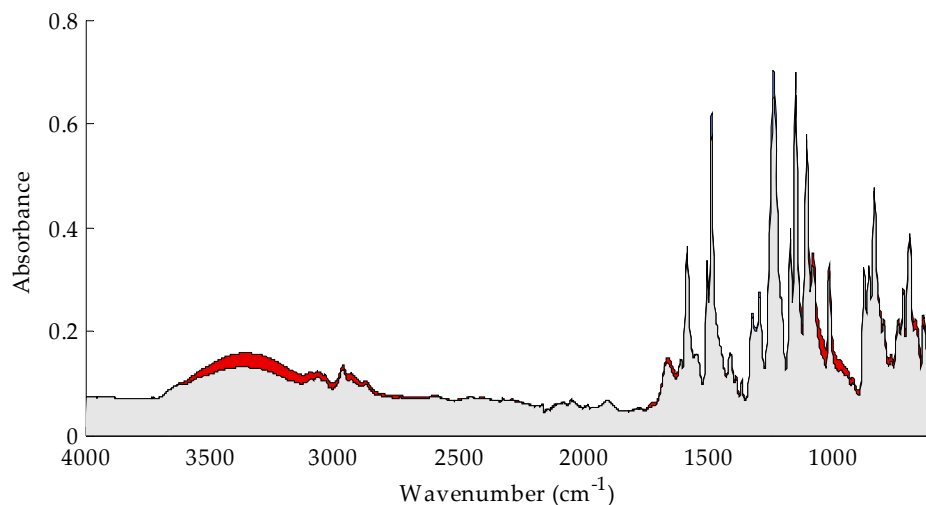


Figure 3.12. ATR-FTIR spectra from the fouled Hydranautics SWC4 membrane coupon run with West Basin seawater at UIUC.

3.3.2 Foulant Analysis of Tampa Bay Seawater

SEM images of Hydranautics SWC4 (UIUC sample) membrane fouled with Tampa Bay seawater are shown in Figure 3.13. The surface coverage of the foulant layer on the membrane surface is nonuniform. No granular areas were observed in scanning of large areas of the membrane. EDS analysis performed on the membrane is shown in Figure 3.14. The EDS analysis showed small amounts of iron in the film.

The AFM image obtained from a Hydranautics SWC4 membrane fouled with Tampa Bay water is shown in Figure 3.15. The surface seems to be very flat, and the membrane surface topography can be faintly seen through the film formed on the membrane surface. The roughness values measured also indicate a flat film morphology; namely, significantly lower RMS roughness than found for the the clean membrane surface (RMS roughness ~ 150 nm).

Figure 3.16 shows the ATR-FTIR spectra for a Hydranautics SWC4 membrane fouled with Tampa Bay seawater. Similar to West Basin seawater, absorbance spectra at 890 to 1050, 1620 to 1680, and 3000 to 3600 cm^{-1} were dominant, representing polysaccharide-like material present on the foulant layer. Personal communication with TBDP revealed that organic fouling was prevalent at the full-scale facility and that chemical cleaning was performed every 2 to 3 months. However, the nature of organic foulant deposited at the full-scale facility is not known.

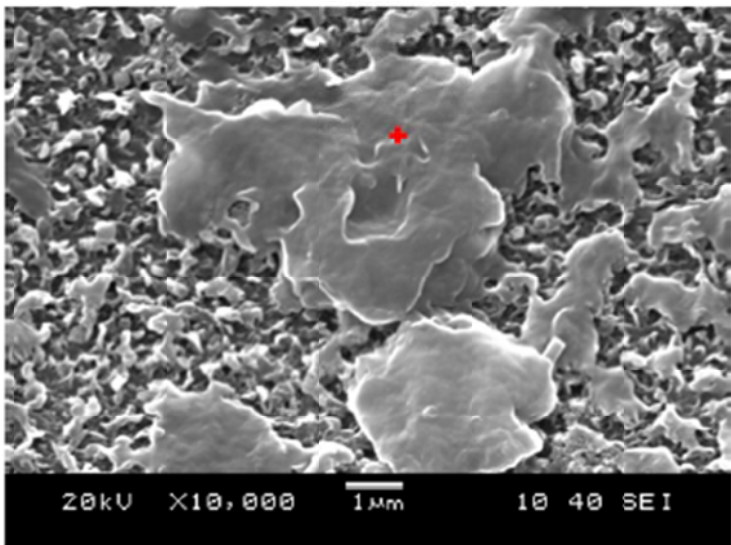


Figure 3.13. SEM image of Hydranautics SWC4 membrane fouled by Tampa Bay seawater.

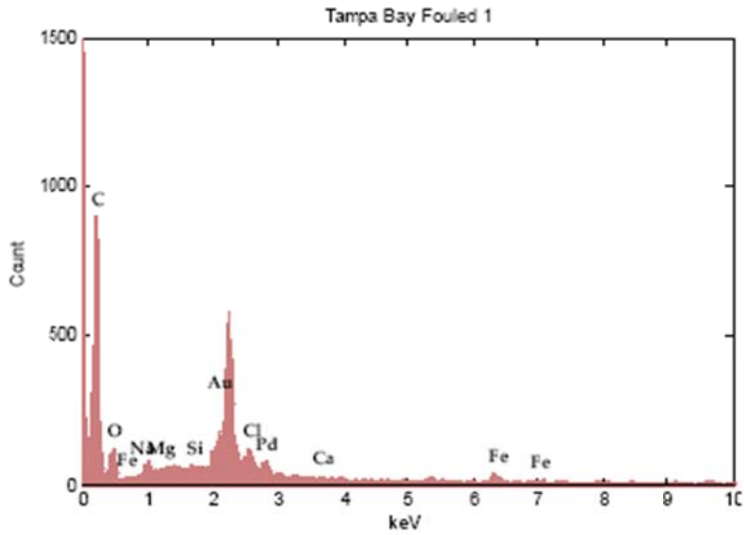


Figure 3.14. EDS analysis of Tampa Bay seawater-fouled Hydranautics SWC4 membranes.

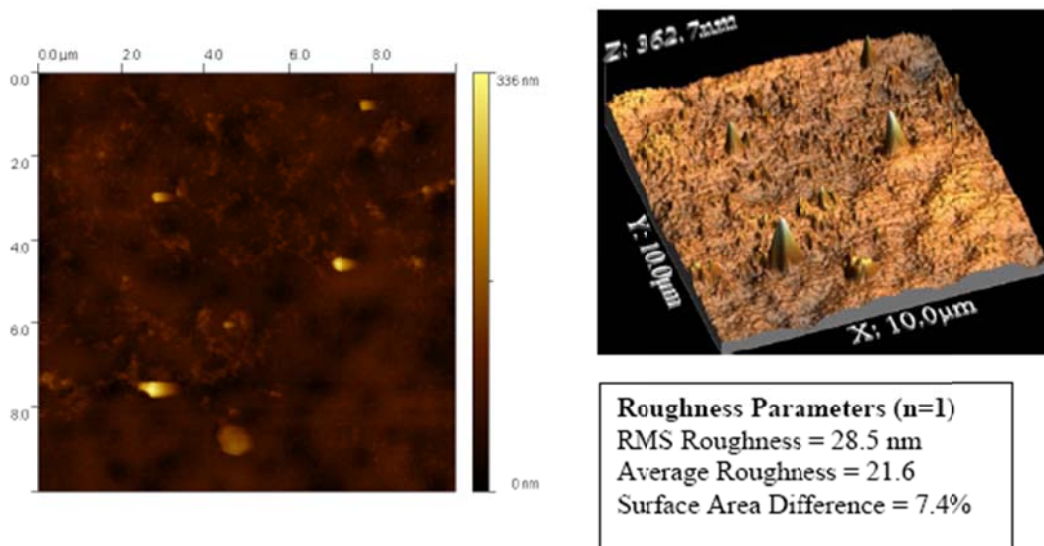


Figure 3.15. AFM topograph of Hydranautics SWC4 membrane fouled with Tampa Bay seawater and roughness parameters.

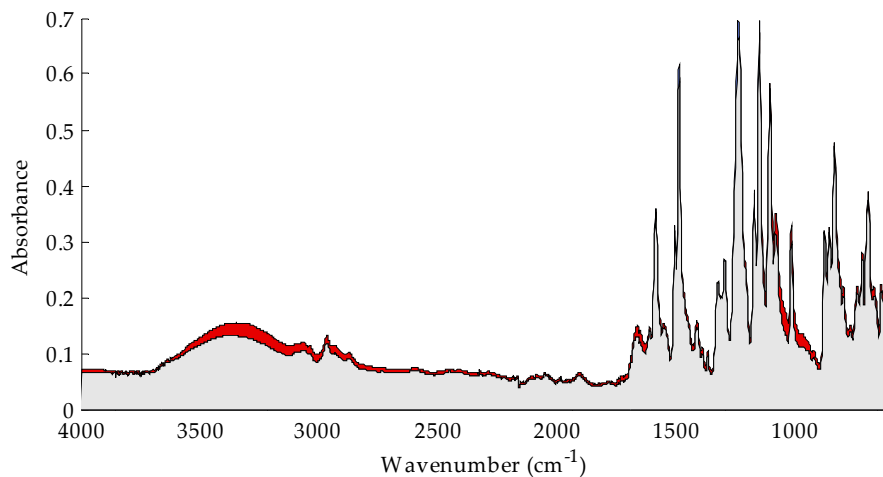


Figure 3.16. ATR-FTIR spectra from the fouled membrane coupon run with Tampa Bay seawater at UIUC.

3.3.3 Foulant Analysis of Carlsbad Seawater

Analysis of the fouled RO membranes operated on Carlsbad seawater was conducted at both the MWH site and the UIUC site. MWH tests showed higher fouling potential than seen at UIUC. SEM images of the fouled membrane (MWH sample) obtained after bench-scale experiments conducted using Hydranautics SWC4 membranes are shown in Figure 3.17, and the EDS analysis is shown in Figure 3.18. The SEM image shows a crusty material covering large areas of the membrane. EDS analysis performed on these areas shows the presence of a variety of metals that originated from the corrosion of the brass pumps and steel components of the system. The metals detected on the membrane surface include iron, copper, and possibly zinc and chromium. These results may represent conditions where extensive corrosion of materials might be occurring in SWRO systems because metals were below detection limits in the raw seawater obtained from Carlsbad (Table 3.1).

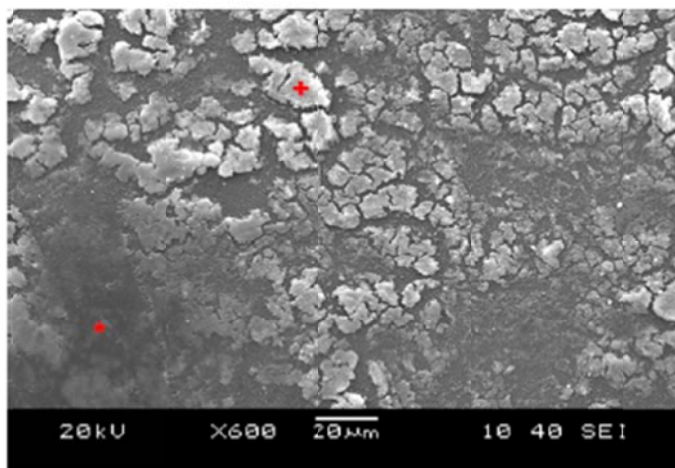


Figure 3.17. SEM image of Carlsbad fouled Hydranautics SWC4 membrane (MWH sample).

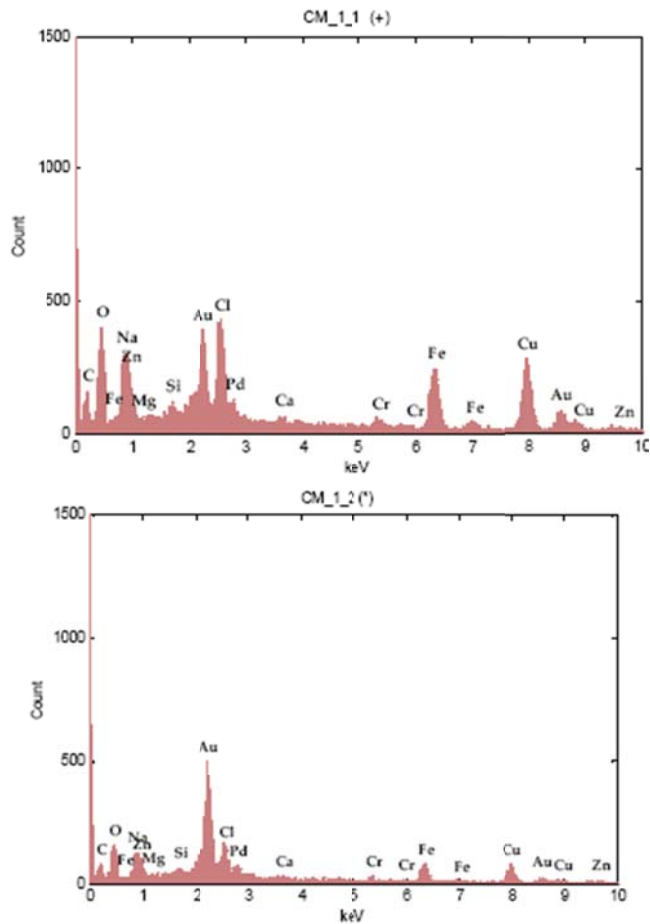


Figure 3.18. EDS analysis of Carlsbad-fouled Hydranautics SWC4 membrane (MWH sample).

SEM images of the fouled membrane (UIUC sample) obtained after bench-scale experiments conducted with Carlsbad water using Hydranautics SWC4 membranes are shown in Figure 3.19, and the EDS analysis is shown in Figure 3.20. SEM images of the fouled membranes show extensive film-covered areas, with some areas covered with granules on the membrane. SEM/EDS of these areas shows the presence of iron in the film similar to other samples. Because of the heterogeneous nature of the fouling layer, AFM images were difficult to acquire and are not shown here.

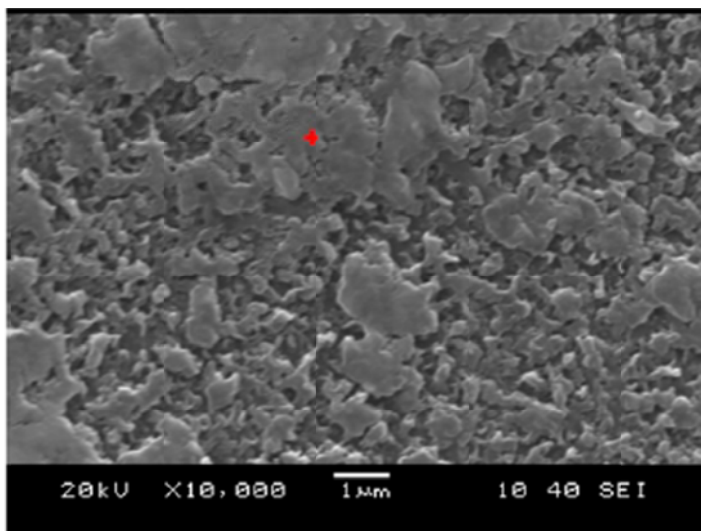


Figure 3.19. SEM image of Carlsbad-fouled Hydranautics SWC4 membrane (UIUC sample).

Absorbance spectra obtained using ATR-FTIR for a fouled Hydranautics SWC4 membrane for experiments conducted at MWH and UIUC are shown in Figure 3.21 and Figure 3.22, respectively. For the Carlsbad seawater run performed at MWH, the foulant intensities are significantly higher than in the three runs at UIUC, indicating more material present in the foulant layer. The regions of highest fouling in the spectra are similar to the UIUC runs, and one would suspect polysaccharide in the foulant layer.

It should be mentioned that clear conclusions about chemical makeup cannot be drawn from ATR-FTIR data. There are many spectral regions where proteins and polysaccharides both absorb IR radiation, and other types of biopolymers could absorb in these regions, as well. Further, inorganic components like OH groups in corrosion products (namely, FeOH_3) can absorb in regions similar to those where polysaccharides absorb (IR behavior is also strongly affected by OH groups). When we interpret the spectra, then, we are looking for general features and overall absorption levels and are not quantifying the exact amounts of the different materials present. To compare the nature of foulant from the bench-scale experiments with pilot-scale testing, an autopsy was performed on a single spiral-wound element used for pilot-testing with Carlsbad seawater. Similar polysaccharide-like material was found on the pilot-scale membrane. A detailed description of the comparison is made in Section 3.6.

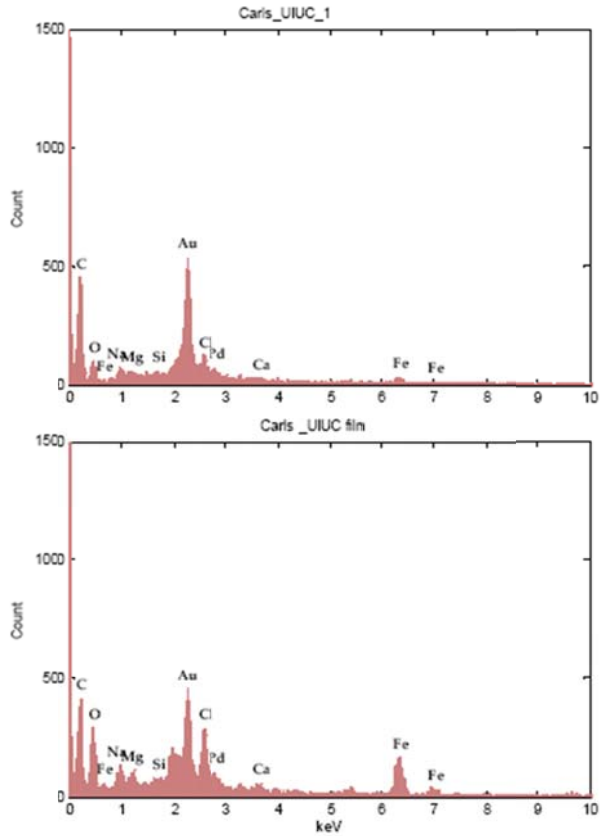


Figure 3.20. EDS analysis of Carlsbad-fouled Hydranautics SWC4 membrane (UIUC sample).

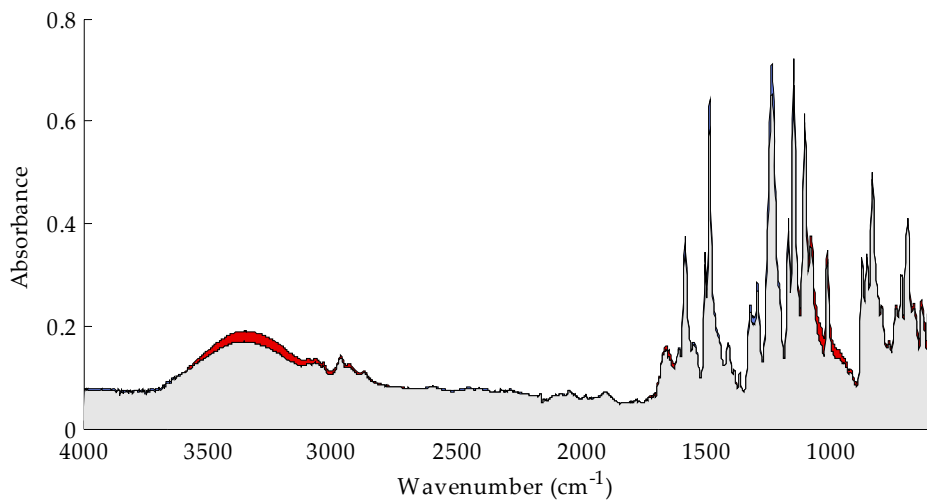


Figure 3.21. ATR-FTIR spectra from the fouled membrane coupon run with Carlsbad seawater at UIUC.

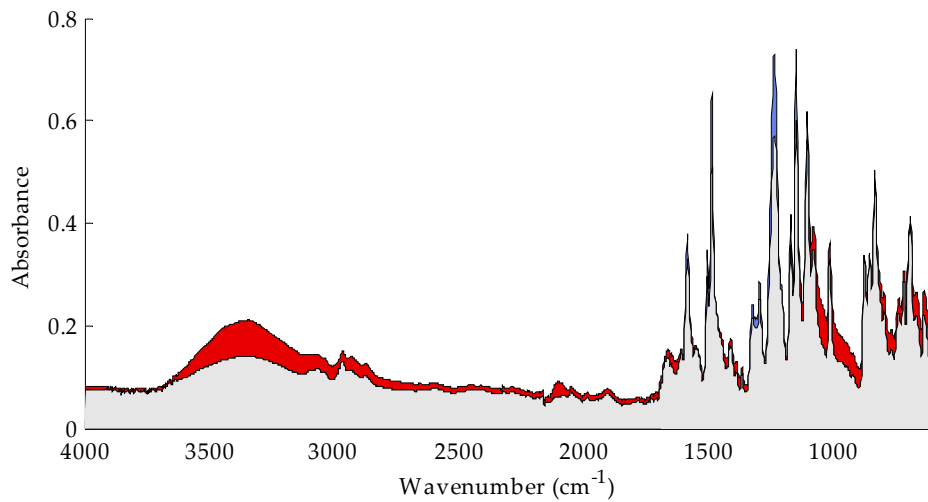


Figure 3.22. ATR-FTIR spectra from the fouled membrane coupon run with Carlsbad seawater at MWH.

3.3.4 Determination of Surface Energy of Foulant Layer

To determine the change in surface energy after fouling, contact angle measurements were performed on Hydranautics SWC4 membranes after bench-scale experiments with West Basin, Tampa Bay, and Carlsbad seawater. The contact angles are shown in Figure 3.23. The contact angles of the apolar liquid (diiodomethane) increased significantly ($\sim 50^\circ$) for the membrane after being filtered with all three source waters when compared to clean membrane diiodomethane angle ($\sim 22^\circ$). Water contact angles decreased significantly when the membrane was tested with Tampa Bay seawater. Contact angles with ethylene glycol also increased significantly when compared to the clean membrane angle ($\sim 12^\circ$).

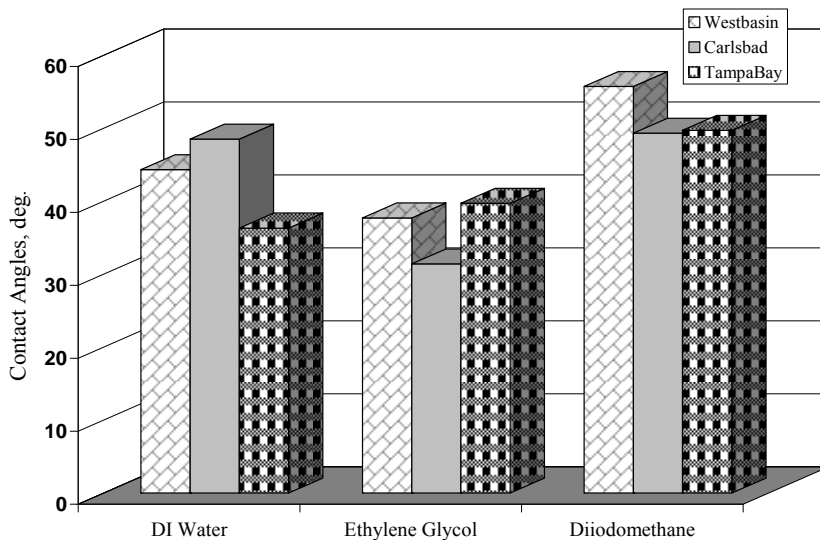


Figure 3.23. Comparison of contact angles using 3 liquids on fouled Hydranautics SWC4 membrane.

The change in contact angles with the three probe liquids was used to determine the surface energy parameters and free energy of cohesion of the modified membrane and is listed in Table 3.4. The electron-donor component (γ^-) component of the free energy for the fouled SWC4 membrane significantly increased when compared to results for the clean membrane. The electron-donor component for the clean membrane was about 13 mJ/m² (Table 3.3), whereas for the Hydranautics SWC4 membrane after fouling with the three source waters, it was more than 35 mJ/m². This result suggests that a significant amount of electron-donor functionalities (such as COO⁻ groups) present on the foulant layer led to the difference in contact angles. The free energy of cohesion is positive for all the three modified membranes, suggesting that the nature of foulant deposited on the membrane surface is hydrophilic. The free energy of cohesion was - 25 mJ/m² (negative) (Table 3.3) for the clean membrane, whereas for the modified membranes, it was > 11 mJ/m² (positive).

Table 3.4. Surface Energy Parameters (mJ/m²) for Fouled Hydranautics SWC4 Membrane

Location for Foulant in Seawater	Values for:			
	γ^w	γ^+	γ^-	ΔG^{CO}
West Basin	31.1	0.3	44.5	27.7
Carlsbad	34.6	0.5	34.4	11.3
Tampa Bay	34.5	0.0	56.6	47.0

From this analysis of the membrane coupons, it is clear that the surface property of the membrane has been altered significantly. Surface functionality and roughness changed significantly, proving the deposition of foulants on the membrane surface. Although a decrease in specific flux was not evident from the bench-scale studies, use of the analytical techniques described earlier can be helpful in determining the nature of seawater foulants. Once the foulants present in seawater are deposited on the membrane surface in multilayers to significantly alter the clean membrane surface properties, interaction between the foulant and the foulant-modified membrane will dominate fouling behavior. A simplified illustration of a fouling mechanism for clean and modified membranes is shown in Figure 3.14.

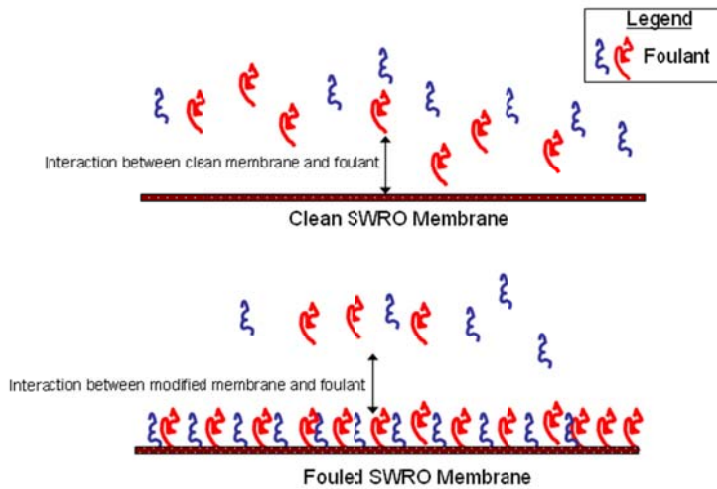


Figure 3.24. Illustration of interaction between seawater foulant and clean/modified membrane.

3.4 IMPACT OF MEMBRANE TYPE ON FOULING

Influence of membrane properties on fouling was studied using Hydranautics SWC4 and DowFilmtec SW30HR membranes. Initial studies were performed with South Bay seawater, and the normalized specific flux for the two membranes is shown in Figure 3.25. From previous experience it was found that operating the bench-scale system longer than 10 h led to corrosion issues. Thus, the experiment was conducted for only 6 h. Also, because a significant decline in specific flux was not obtained for the three seawater sources (West Basin, Tampa Bay, and Carlsbad), seawater from South Bay was used for this study. The normalized specific flux decline was slightly higher for the rough and hydrophobic membrane (Hydranautics SWC4) than for the smooth and hydrophilic membrane (DowFilmtec SW30HR). Although a slightly lower normalized specific flux for DowFilmtec SW30HR membrane was observed, it is not clear if the results are significantly different. In general, smooth and hydrophilic membranes exhibit lower fouling potential than do rough and hydrophobic membranes (Elimelech et al., 1997). When the surface of the membrane is hydrophilic, water molecules form its natural structure through hydrogen bonding. Because of the high electron component (γ^-) of the DowFilmtec SW30HR membrane, hydrophilic repulsion between the organic foulant and the membrane surface leads to less deposition and a smaller decrease in normalized specific flux. When the membrane surface is hydrophobic, water experiences a repulsive force that disturbs the natural water structuring on the membrane surface and leads to hydrophobic attraction between the foulant and membrane surface.

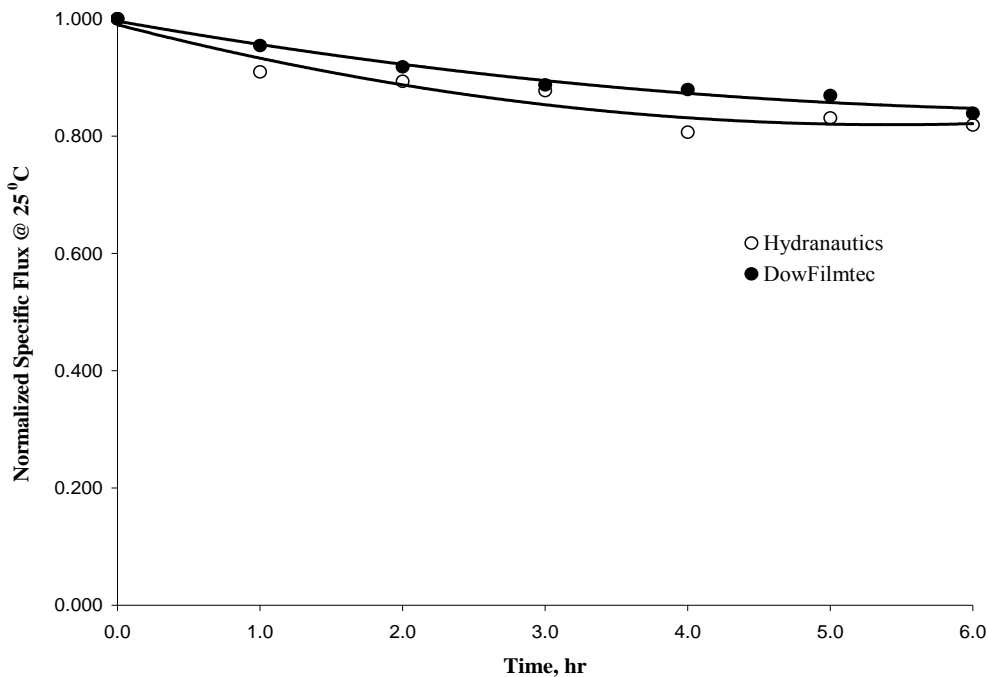


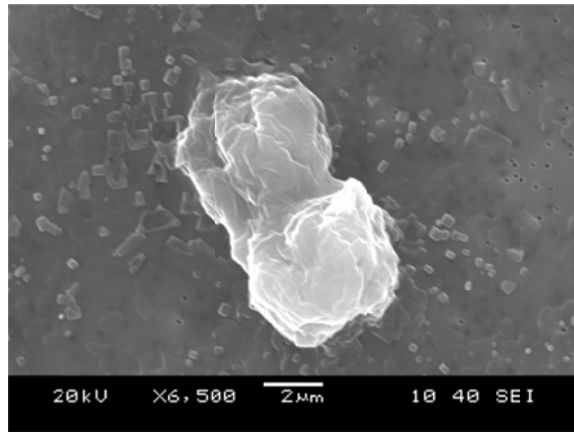
Figure 3.25. Comparison of normalized specific flux for Hydranautics SWC4 and DowFilmtec SW30HR membranes with South Bay seawater.

3.5 IMPACT OF AOM FOULING

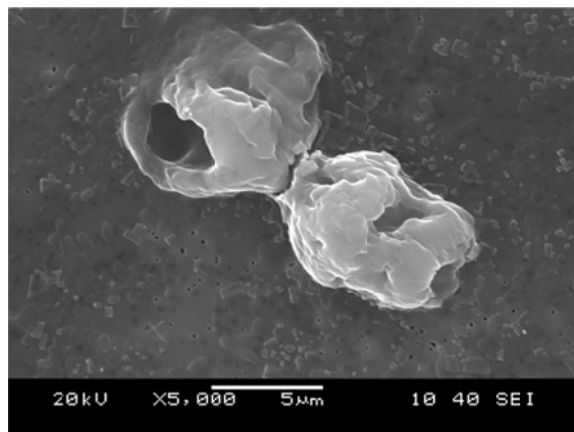
To determine the influence of membrane type and AOM fouling in the feed water, bench-scale experiments were conducted using *H. pygmaea* cells. SEM images of *H. pygmaea* are shown in Figure 3.26. In Figure 3.26a, a typical cell is shown; the double-sectioned body is fairly standard morphology. In Figure 3.26b, two cells are connected, possibly because of incomplete cell division. One of the cells' structure has been compromised. In Figure 3.26c, an intact cell sits beside a mass of material that appears to be a second, broken cell. It is presumed that the small jagged clusters are organelles that were released upon cell lysis. Such lysis and release of organic matter might occur during a spike of phytoplankton entering the RO unit.

To determine the influence of membrane properties, both Hydranautics SWC4 (rough, hydrophobic) and DowFilmtec SW30HR (smooth, hydrophilic) membranes were used. Because the Saehan SR membrane did not have significant differences in surface properties (roughness and hydrophobicity) from the Hydranautics SWC4 membrane, results were compared only for Hydranautics SWC4 and DowFilmtec SW30HR membranes with no pretreatment. Normalized specific flux for the two membranes is shown in Figure 3.27. No significant difference in the normalized specific flux was observed for the two membranes. But the normalized specific flux decreased with time for both membranes.

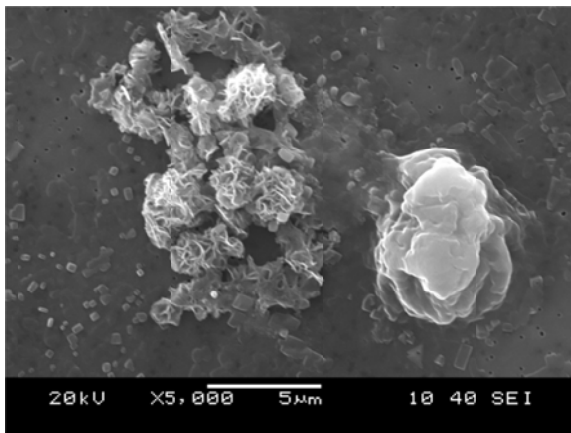
After the initial run with *H. pygmaea* cells, the feed water was prefiltered through an MF membrane. A comparison of normalized specific flux for the Hydranautics SWC4 and DowFilmtec SW30HR membranes is shown in Figure 3.28. No significant difference in the normalized specific flux was observed for the two membranes. Hence, prefiltration with an MF membrane removed a large fraction of the AOM and led to minimal decline in specific flux.



(a)



(b)



(c)

Figure 3.26. SEM images of *H. pygmaea* cells.

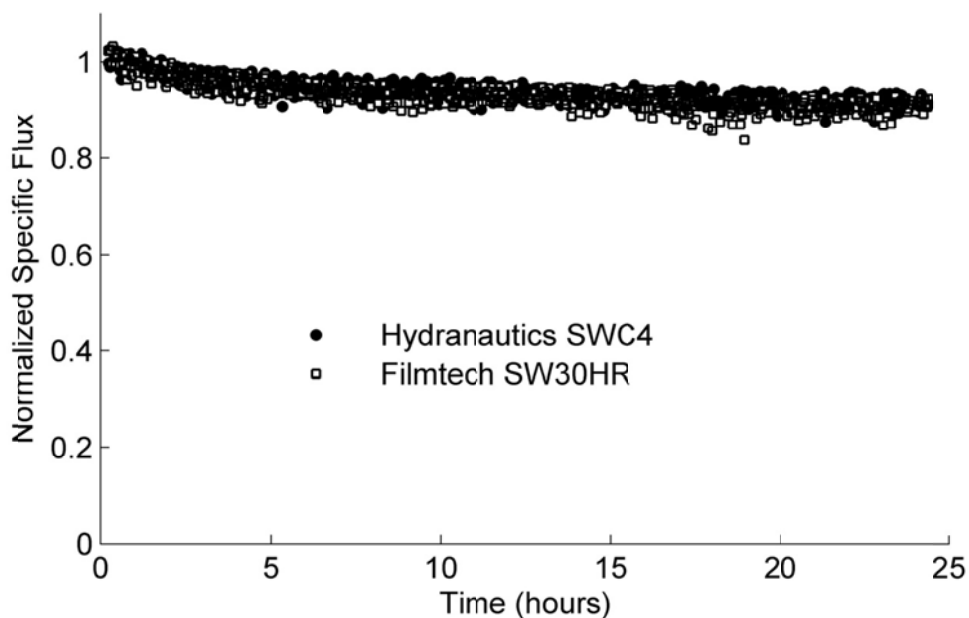


Figure 3.27. Normalized specific flux decline comparison for Hydranautics SWC4 and DowFilmtec SW30HR membranes with *H. pygmaea* cells with no prefiltration.

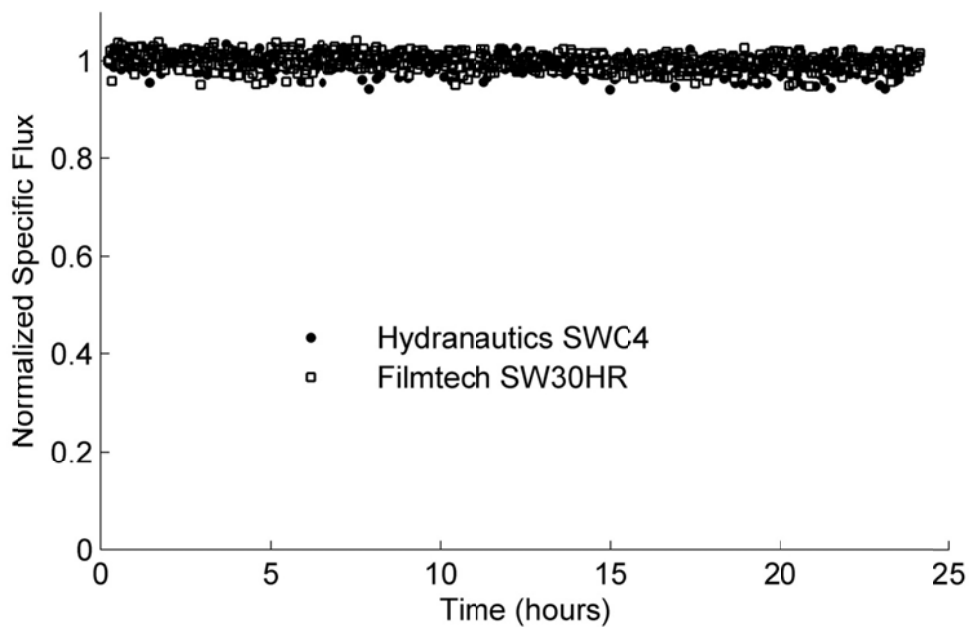


Figure 3.28. Normalized specific flux decline comparison for Hydranautics SWC4 and DowFilmtec SW30HR membranes with *H. pygmaea* cells with pre-MF.

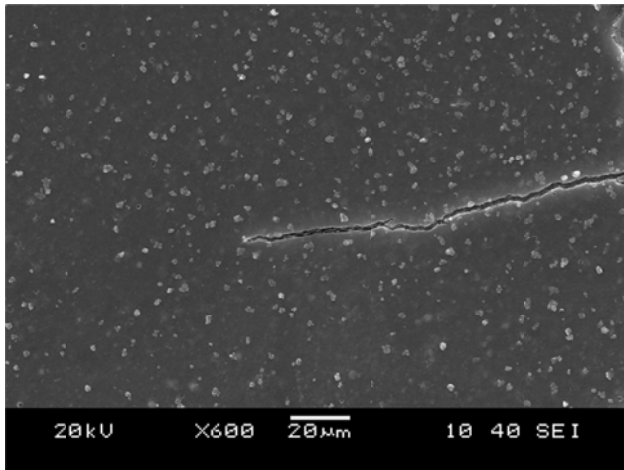
When *H. pygmaea* cells and the derived AOM were used, no difference in flux decline was observed when two membranes with significantly different roughness and hydrophobicity were used. Nanoscale roughness and hydrophobicity of the membrane surface alter the physicochemical interactions, such as van der Waals, electrostatic, and acid–base forces

between the foulant and membrane surface. All the physicochemical interactions are a function of size of the foulant particle. In the case of *H. pygmaea* cells, the average diameter of the cells is $\sim 20 \mu\text{m}$, and hence hydrodynamic forces (crossflow velocity) play a more significant role than short-range physicochemical interactions. Inertial lift is dominant for particles exceeding $20 \mu\text{m}$ in diameter, and shear-induced diffusion is dominant for particles in the size range of $1\text{--}20 \mu\text{m}$. Because the cells were shearing during the experimental study, a combination of inertial lift and shear-induced diffusion can cause the *H. pygmaea* cells to transport away from the membrane surface and hence avoid deposition. Digital images of the fouled membrane surface when *H. pygmaea* cells were used are shown in Figure 3.29. Only the fouled Hydranautics SWC4 membrane is shown. There is a significant amount of brown alga-derived deposit on the surface.

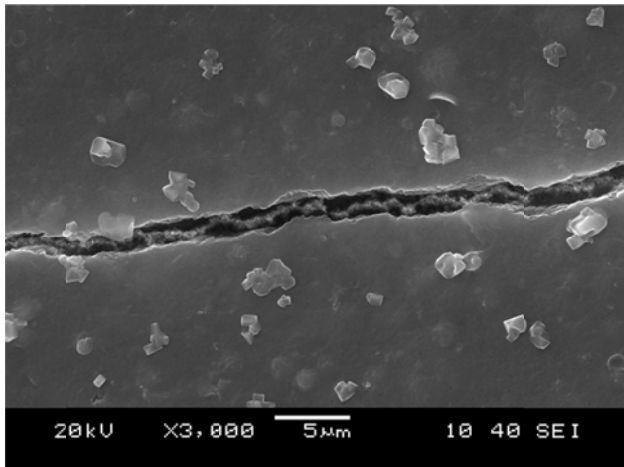
SEM images at various magnifications when *H. pygmaea*-spiked water was used are shown in Figure 3.30 for Hydranautics SWC4. No whole cells are visible in the images, confirming the dominance of back transport velocity in preventing deposition of cells on the membrane surface. Only the organic matter released from the cells is present on the surface, which forms a cake (gel) layer on the membrane surface. The cake layer is thick, and the underlying membrane cannot be seen.



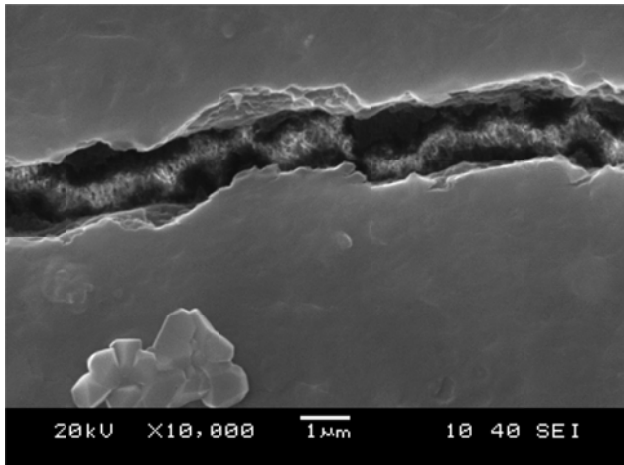
Figure 3.29. Digital images of fouled Hydranautics SWC4 membrane when *H. pygmaea*-spiked water was used without prefiltration.



(a)



(b)



(c)

Figure 3.30. SEM images of fouled Hydranautics SWC4 membrane at (a) 600 \times , (b) 3000 \times , and (c) 10,000 \times magnifications when *H. pygmaea*-spiked water was used without prefiltration.

When prefiltration with MF membrane was used, no difference in normalized specific flux was obtained between the two membranes (Figure 3.28). Membrane surface properties play a key role until a monolayer of foulant is deposited on the membrane surface. Once a layer of foulant covers the membrane surface, there is no interaction between the clean membrane surface and the foulant. Because more than 40,000 cells/mL were used during the study, a significant concentration of AOM would be released by shearing. Hence, within a short interval, a multilayer deposition of organic matter on the membrane surface is achieved and no difference in normalized specific flux is observed.

To determine the deposit layer on the two membrane surfaces, digital images and SEM images were generated. When the water was filtered by using an MF membrane to remove the *H. pygmaea* cells prior to a subsequent fouling study, no deposits were seen on the digital images (Figure 3.31). The SEM images at various magnifications for Hydranautics SWC4 are shown in Figure 3.32. Foulant material was present on the membrane surface, but the coverage was not complete. When MF-pretreated water was used, uneven deposition of foulant occurred on the membrane surface. Hence, no cake layer was formed on the membrane surface within the time (24 h) of the test. Thus, no substantial change in specific flux between the two membranes occurred. Because deposition of organic matter on the membrane surface is based on adsorption phenomena, the concentration of organics in the feed water would play an important role in determining fouling behavior.

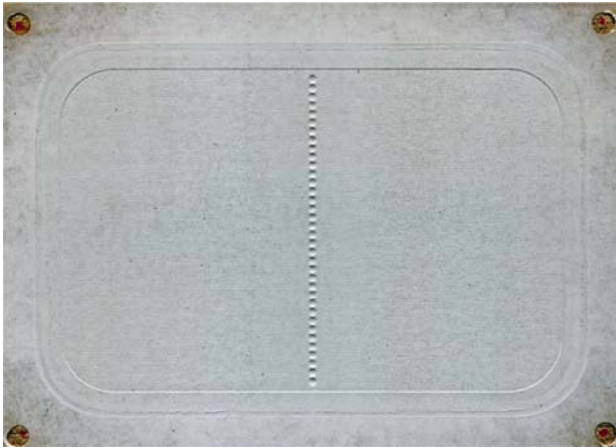
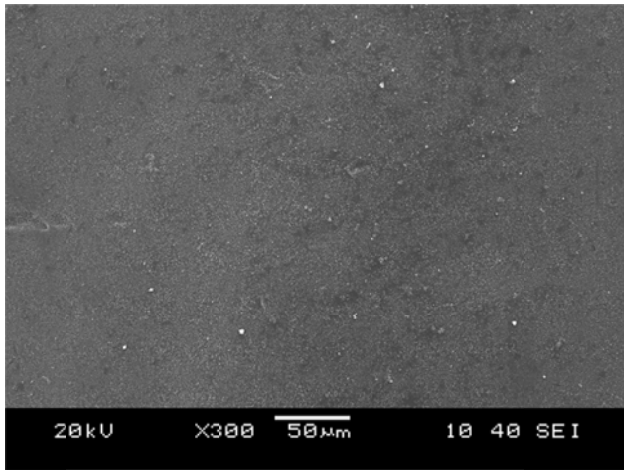
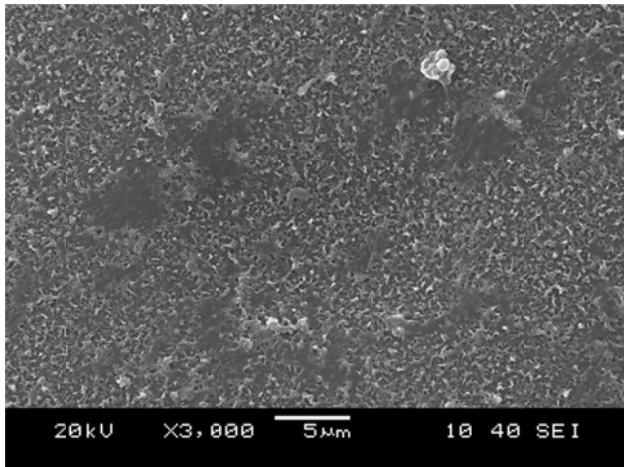


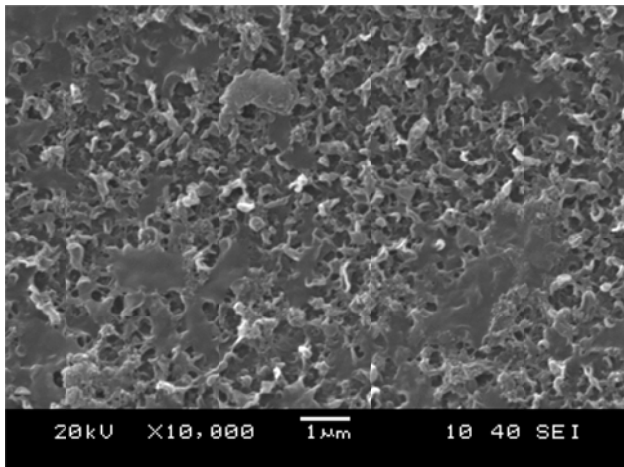
Figure 3.31. Images of fouled Hydranautics SWC4 membrane when *H. pygmaea*-spiked water was used with pre-MF.



(a)



(b)



(c)

Figure 3.32. SEM images of AOM fouling on Hydranautics SWC4 membrane coupon at (a) 600 \times , (b) 3000 \times , and (c) 10,000 \times magnification.

To determine the inorganic constituent present on the foulant layer, EDS analysis was performed. An SEM image of the DowFilmtec SW30HR membrane after algal experiments is shown in Figure 3.33 with the locations (A and B) for EDS analysis. The EDS spectra are shown in Figure 3.34 and Figure 3.35. Peaks for carbon, oxygen, sodium, chloride, calcium, and iron are all stronger at location B than at location A. Greater strength could be caused by a stronger signal coming from the surface of the foulant as opposed to a weaker signal received from the crack in the foulant layer. It is also important that iron was present even in this very thick cake layer. Iron could be from corrosion in the system, or it could be from the algal cells themselves, which incorporate iron as part of their photosynthetic machinery.

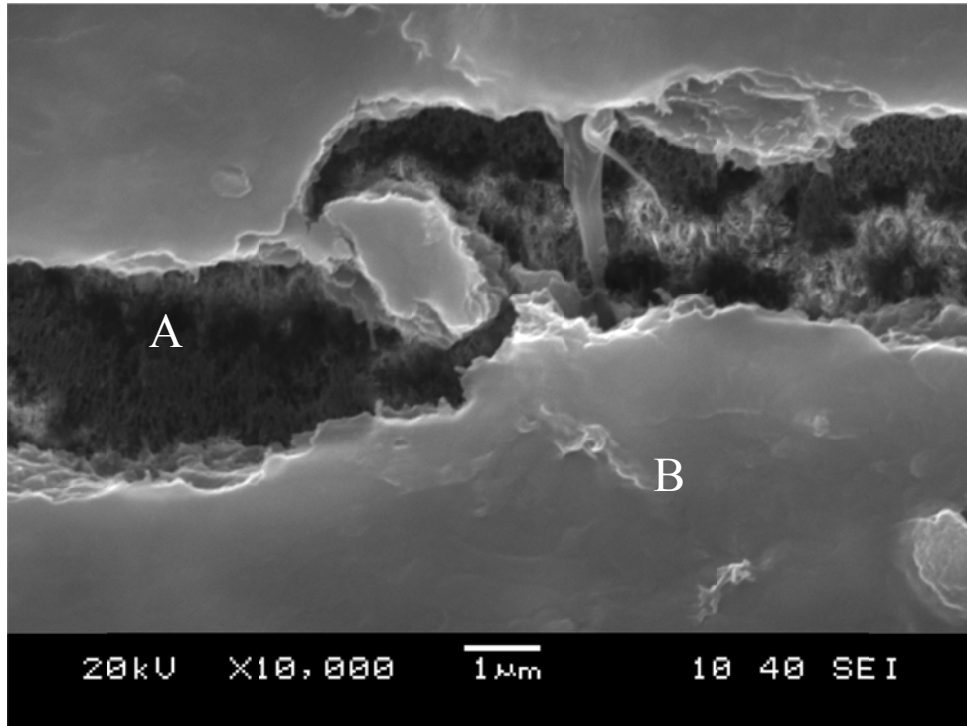


Figure 3.33. SEM image of DowFilmtec SW30HR membrane after AOM fouling experiment. Locations A and B were chosen for EDS analysis.

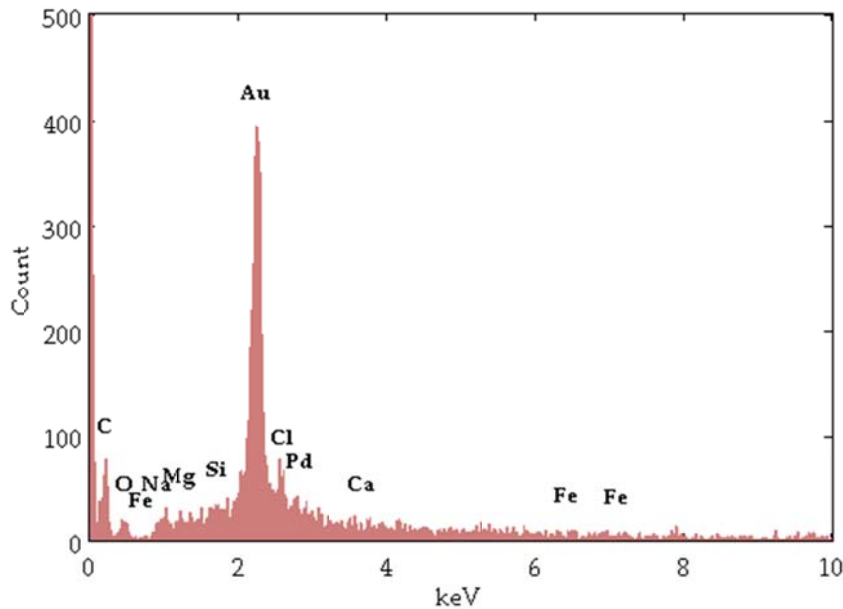


Figure 3.34. EDS spectrum at location A in the SEM image shown in Figure 3.33.

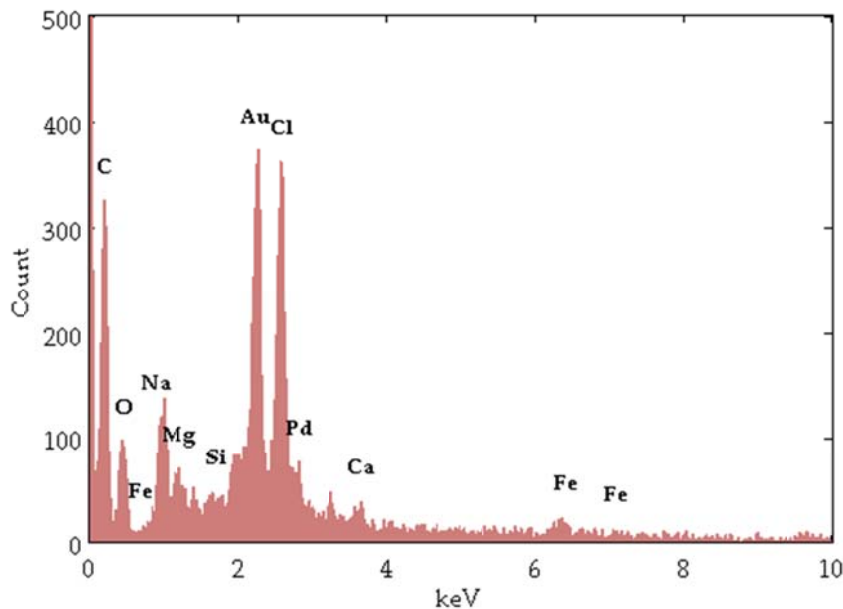


Figure 3.35. EDS spectrum at location B in the SEM image shown in Figure 3.33.

ATR-FTIR analysis was performed on the membranes. In Figure 3.36, infrared absorbance spectra in the region of 3700 to 2600 cm^{-1} are shown. The NaCl compaction test is included as a reference. The membranes tested with microfiltered AOM accumulated significant levels of foulant material. The absorbance at 3300 cm^{-1} for microfiltered AOM on the Hydranautics SWC4 membrane was 25% of the absorbance for the *H. pygmaea* spike foulants (when the absorbance is zeroed at the level of the NaCl compaction test). For DowFilmtec SW30HR membranes, the absorbance of microfiltered AOM was 39% that of the *H. pygmaea* spike. It is interesting, however, that there was no measurable flux decline in either of the

microfiltered AOM runs. This shows that flux in bench-scale RO tests is not easily diminished by organic material deposited on the membrane. The spectra were similar in different locations on the membrane surface. The magnitude of the spectra was different at various locations because of more foulant accumulation near the feed spacers. Because of stagnation zones present near the feed spacers, more foulant deposition occurred and hence magnitudes of spectra obtained in the region near the feed spacers were high.

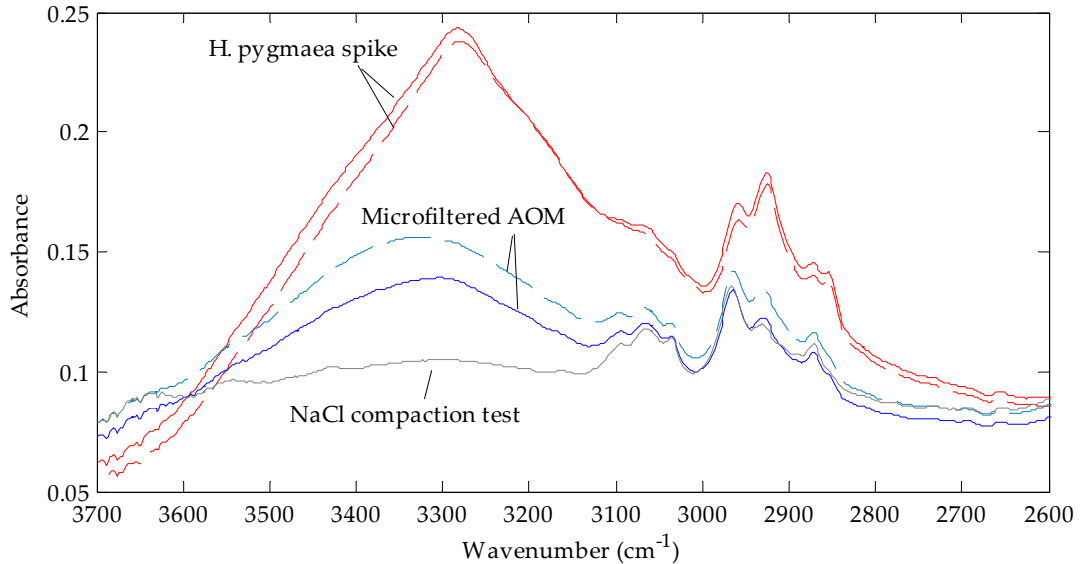


Figure 3.36. Infrared absorbance spectra in the region of 3700 to 2600 cm^{-1} for Hydranautics SWC4 (solid line) and DowFilmtec SW30HR (dashed line) after experiments with *H. pygmaea* water with/without prefiltration.

3.6 COMPARISON OF BENCH-SCALE AND PILOT-SCALE FOULING

In order to compare bench-scale experimental results with pilot plant results, a lead element from the Carlsbad pilot plant was removed and an autopsy conducted. The pilot plant at Carlsbad was operated using a Hydranautics SWC4+ membrane for a period of about 2 weeks at ~ 8 gfd of flux. The pilot plant operated for only a short period because of significant metallic fouling that occurred within 2 weeks of operation. The SEM results obtained from the pilot scale membrane operated on Carlsbad seawater are shown in Figure 3.37. The images show a film on the membrane with the membrane visible through holes in this film (as seen in the 10,000 \times image) and in uncovered areas (3,000 \times image). EDS results are shown in Figure 3.38. The EDS spectrum of this fouling layer is very similar to those obtained with the same water and a similar membrane from bench-scale tests at UIUC (Figure 3.20), indicating that the fouling conditions and early-stage film formation were captured in the bench-scale tests. As expected, the film in the short-term bench-scale tests (24 h) seems thinner than the film on membranes used in the longer pilot studies (2 weeks)

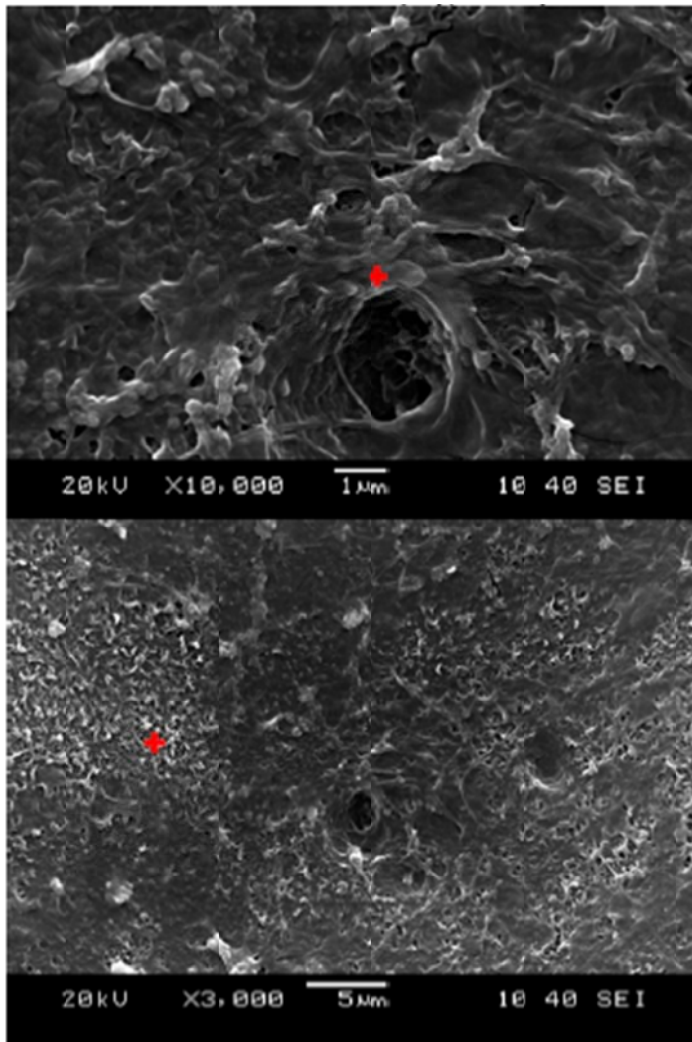


Figure 3.37. SEM image of lead element from the Carlsbad pilot plant.

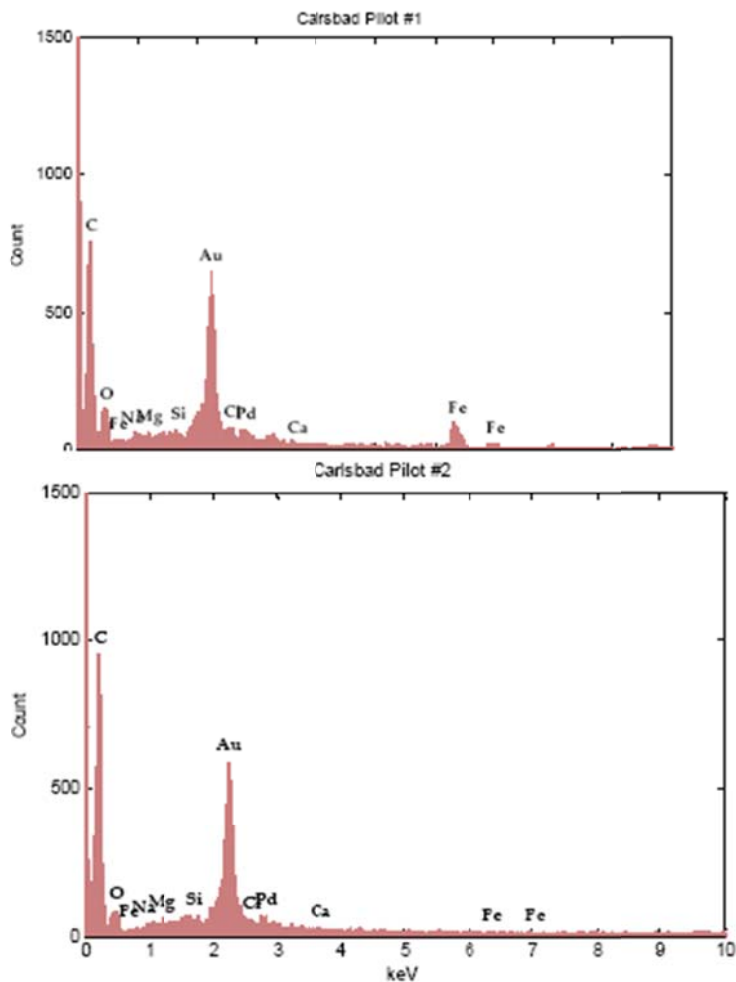


Figure 3.38. EDS analysis of lead element from the Carlsbad pilot plant.

ATR-FTIR analysis was used to compare the surface functionality of the pilot and bench-scale foulant layers. Figure 3.39 presents ATR-FTIR data from the autopsy of a Hydranautics SWC4+ membrane module used in the Carlsbad seawater desalination pilot facility. Five different locations on each of the coupons were measured and averaged. Red indicates areas where the unrinsed sample had higher absorbance. Blue indicates areas where the rinsed sample showed higher absorbance (foulant material had a “blocking” effect in these IR frequencies). Grey indicates overlap. For comparison, spectra from protein (dry bovine serum albumin pressed against the ATR crystal) and polysaccharide (dried sodium alginate gel) are shown. The peaks obtained are similar to those from bench-scale studies (Figure 3.21 and Figure 3.22). The “peaked” appearance of the fouled membrane spectrum around 3300 cm^{-1} could be indicative of proteins in the foulant layer. This theory is consistent with the dual peaks at 1540 and 1640 cm^{-1} . However, polysaccharides are also strongly indicated by the elevated absorbance of the foulant material in the region of 1000 cm^{-1} .

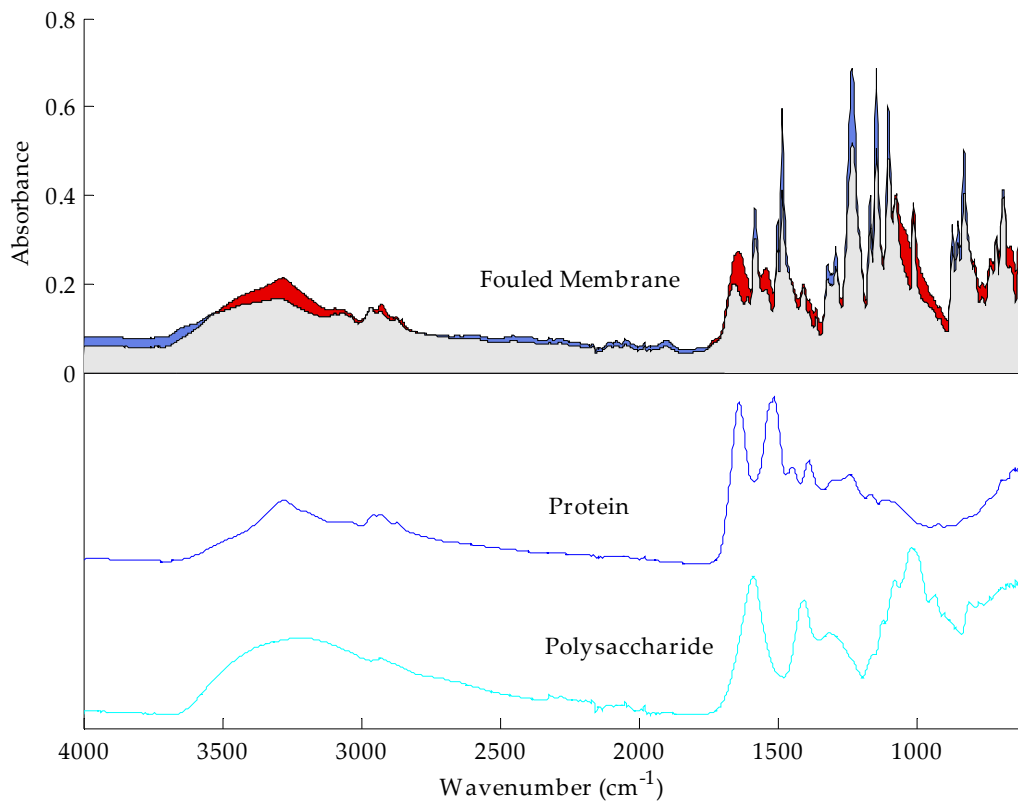


Figure 3.39. ATR-FTIR spectra from the autopsy of a Hydranautics SWC4+ membrane module used in the Carlsbad seawater desalination pilot facility.

3.7 APPLICABILITY OF ANALYTICAL METHODS FOR SWRO PROCESSES

A summary of all the techniques used to characterize the seawater, membrane, and foulant is given in Table 3.5. Certain methods, such as absorbance, TOC, and HPSEC measurements, are for characterizing the seawater, and methods such as streaming potential, AFM, contact angles, ATR-FTIR spectroscopy, SEM, and EDS are for characterizing clean and fouled membrane surfaces. The applicability of each analytical method is described in the following:

Absorbance measurements: Carbohydrate and polysaccharide content in the seawater can cause fouling of the SWRO membrane, leading to a decline in the membrane performance. Absorbance measurements at 595 nm can be utilized to determine the carbohydrate and polysaccharide content present in a seawater source. It is difficult to correlate the concentration of organic matter with fouling potential on the SWRO membrane because various factors, such as pretreatment process, membrane type, RO system configuration, and hydrodynamics, affect the extent of fouling. Nevertheless, estimation of the concentration of carbohydrate and polysaccharide content in a seawater source will help in determining the nature of organic matter present.

TOC: Estimation of TOC content of a seawater source can be used to determine the extent of biological activity. Seawater with higher biological activity (during algal blooms) will

exhibit higher TOC concentrations. The fouling potential of a given source seawater changes over time and with various events occurring in the ocean (such as red tides, spring swells, rain events, etc.). Thus, continuous monitoring of water quality parameters such as TOC in addition to turbidity and chlorophyll content is necessary to establish biological activity in the seawater used for intake. A disadvantage with TOC measurements is the interference of the method with high chloride content present in seawater. Catalytic combustion and chemiluminescence detection methods have been developed specifically for seawater TOC analysis (Shimadzu Corporation, 2010). The new method utilizes a combustion tube that can be used three or four times before being exchanged. Catalyst can be regenerated externally and used for a longer period. Such methods can be utilized for accurate measurement of TOC in seawater.

HPSEC: In addition to the determination of the concentration of organic matter using absorbance and TOC measurements, characterization of the organic matter based on size will help in choosing an efficient pretreatment process. HPSEC measurements can be utilized to characterize the size fraction of organic matter present in seawater. Based on the size range of organic matter, conventional and membrane pretreatment processes can be evaluated and optimized.

Streaming potential: Determination of the surface charge of the RO membrane can provide valuable insights on the influence of electrostatic interactions with respect to fouling. The typical method used to estimate the surface charge of membranes is the application of a streaming potential analyzer. Because the ionic strength of seawater is high, streaming potential measurements are not effective. In this study, although streaming potential measurements were different for the membranes under lower-ionic-strength conditions, at an ionic strength of more than 0.1 M, measurements were not different for the model membranes. Thus, other methods for determination of surface charge need to be evaluated to accurately estimate the surface charge of RO membranes under conditions relevant to seawater chemistry. Once the membranes are fouled, it is difficult to use techniques such as streaming potential measurements, as the foulant layer will not stay intact when suspended in the electrolyte used for the analysis.

AFM: In this study, determination of surface roughness using AFM was performed with the tapping mode. Membrane polymers swell because of hydration; hence, roughness measurements could be different under hydrated conditions. The AFM measurements can be useful in determining deposition of foulant material on the membrane surface. A change in the roughness of the membrane after fouling can be interpreted as deposition of foulant material. The use of AFM measurements to determine foulant deposition is limited. Measurements cannot be used to evaluate the nature of the foulant deposited; furthermore, the technique requires skilled labor, and interpretation of results requires sufficient expertise.

Contact angles: In this study, contact angle measurements were performed to determine the relative hydrophobicity and surface energy parameters of clean and fouled membrane surfaces. Surface energy parameters can be utilized to study the influence of RO membrane surface chemistry on fouling. The contact angle measurement technique can also be used to determine the relative hydrophobicity of foulant material.

ATR-FTIR spectroscopy: The organic functionality of the foulant layer can be analyzed using ATR-FTIR spectroscopy. ATR-FTIR spectroscopy is a microscopic measurement technique, and output signals depend on the extent of foulant surface coverage on the membrane. In ATR-FTIR measurements, wavelength from the membrane polymer and the

presence of liquid can interfere with the analysis, making it difficult to differentiate overlapping of IR absorbance for various functional groups. In this study, the technique was effective in determining the presence of protein-like and polysaccharide-like material deposited on the SWRO membrane.

SEM and EDS: SEM and EDS are techniques that are typically used in combination. Observation of membrane surface morphology and of the foulant layer using SEM is well-developed and straightforward. When the foulant layer is biological in nature (such as biofilms), modifications in the technique need to be applied. One such variation is the use of an environmental SEM for characterizing the foulant layer without causing damage to it. EDS is used to determine the inorganic content of a foulant layer. Although precipitation of sparingly soluble salts is not expected in SWRO processes because of low feed water recovery rates, the EDS technique can be used to determine if iron oxide fouling has occurred on the SWRO membrane.

Various steps involved in the comparison of organic fouling of different seawater sources are illustrated in Figure 3.40. Basic water quality analysis involving the measurement of pH, turbidity, and fluorescence would be the first step. Prefiltration of the raw seawater source with a 0.45- μm -pore-size filter will remove particulates from the source water and allow dissolved organics to pass through. The SDI values obtained will give an indication of the extent of particulates present in the seawater. Further analysis using image processing and ATR-FTIR techniques can be used to describe the nature of particulates present. After prefiltration, a detailed water quality analysis involving major ions, bacterial and algal count, TOC, and polysaccharides needs to be performed. Bench-scale experiments with a single membrane type and seawater source should be performed after the prefiltration step. Bench-scale experiments would include equilibration involving compaction of the membrane, followed by the actual fouling run. After bench-scale experiments are complete, an autopsy of the membrane coupon needs to be performed to determine the nature of foulants deposited. Autopsy techniques specifically can be used to determine if the foulants are composed of humics, polysaccharides, proteins, or other organic constituents. Determination of a specific foulant's nature can be used to choose an optimum pretreatment process and to optimize operating conditions for a pilot-scale facility, as well as to identify appropriate cleaning chemicals for removal of deposited foulants.

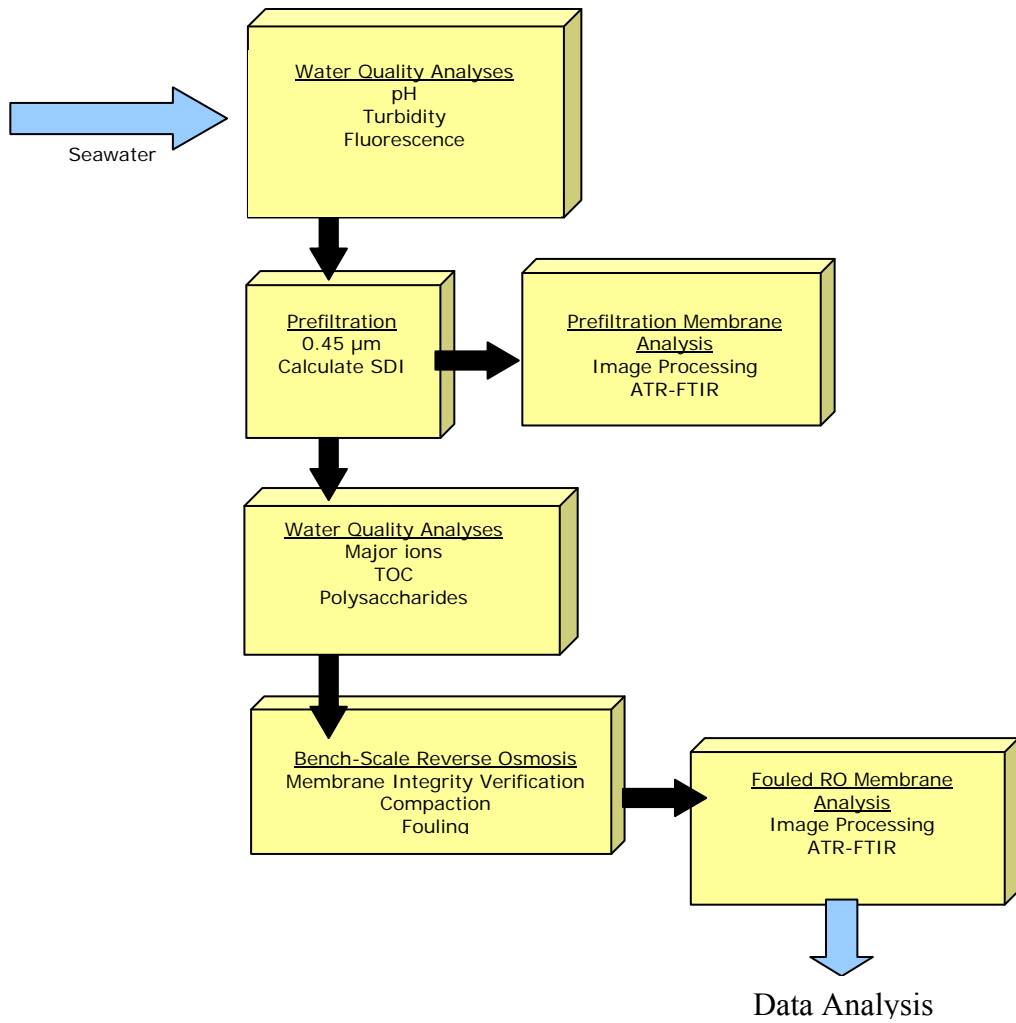


Figure 3.40. Steps to analyze organic fouling potential of different seawater sources.

Table 3.5. Summary of Analytical Methods Used for Characterization of Seawater, Membrane, and Foulant

Technique	Purpose	Application	Advantages	Disadvantages	Results from This Study
Absorbance @ 595 nm	Measurement of carbohydrate content	Seawater characterization	Comparing fouling potential of various seawater sources based on polysaccharide content.	None.	Carbohydrate and polysaccharide content detected in all seawater sources. Concentration and membrane fouling potential could not be correlated.
HPSEC	Measurement of organic size fraction	Seawater characterization	Determining organic size fraction responsible for fouling.	Sensitivity based on detection method used (UV/DOC).	Peaks were found below the lowest detection limit of 1.8 kDa. Organic size fraction and membrane fouling potential could not be correlated.
TOC	Measurement of organic content	Seawater characterization	Comparing fouling potential of various seawater sources based on organic concentration.	Sensitivity issues due to necessary dilution.	Except for Tampa Bay seawater, TOCs for all other seawater sources were below detection limit of 0.5 mg/L.
Streaming Potential	Determination of zeta potential	Clean/fouled membrane characterization	Determining the influence of electrostatic interactions on fouling.	Not efficient for solution ionic strength of >0.1 M. Difficult to measure charge of foulant deposited on membrane (due to foulant desorption).	Zeta potential increased with ionic strength for all the model membranes tested. Zeta potential not representative of membrane surface charge beyond an ionic strength of 0.1 M. Not useful in seawater applications
AFM	Measurement of surface roughness	Clean/fouled membrane characterization	Determining the influence of membrane surface roughness on fouling. Can also be used to determine foulant deposition.	Difficult to measure roughness of fouled membrane (due to interference between foulant and AFM tip).	Surface roughness of Hydranautics membrane higher than that of DowFilmtec and Saehan membranes.
Contact Angles	Determination of surface	Clean/fouled membrane	Determining the influence of	Macroscopic surface	Contact angle of DowFilmtec

Technique	Purpose	Application	Advantages	Disadvantages	Results from This Study
	energy parameters	characterization	membrane surface chemistry on fouling. Can also be used for determining hydrophobicity/hydrophilicity of foulants.	characterization technique. Not sensitive to heterogeneity on membrane surface.	membrane lower than those of Saehan and Hydranautics membranes.
ATR-FTIR	Determination of organic functionality	Clean/fouled membrane characterization	Determining surface functionality of foulant.	Difficult to differentiate overlapping of absorbance for various functional groups.	Fouling due to polysaccharide-like and protein-like material was found on fouled membrane when AOM was added to the seawater source.
SEM	Determination of surface morphology	Clean/fouled membrane characterization	Determining surface morphology of foulant layer and presence of biofilm.	Modification necessary for biological samples.	Surface morphology of clean and fouled membranes revealed foulant structure on membrane. Higher deposition was found when no pretreatment was used with AOM added to seawater source. Presence of iron determined on membrane surface.
EDS	Determination of inorganic functionality	Clean/fouled membrane characterization	Determining surface functionality of foulant.	None.	Presence of iron was due to corrosion of feed water pump used.

Chapter 4

Conclusions and Recommendations

4.1 CONCLUSIONS

In this study, characterization of various seawaters was performed and bench-scale testing done to determine the nature of organic foulants restricting the performance of SWRO membranes. A correlation between seawater characteristics and fouling behavior was not evident from this study as the rate of flux decline was marginal and not significantly different for the various seawater sources tested. However, fouled membrane autopsy results revealed the presence of polysaccharide-like material deposition on the membranes for all the seawater sources tested in this study. The techniques and methods used in this study can be used prior to the operation of a pilot-scale process in order to access the nature of foulant material that would preferentially deposit on the membrane surface.

Characterization of seawater

Three seawater sources from California (Carlsbad, West Basin, and South Bay) and one from Florida (Tampa Bay) were characterized and used in bench-scale experiments to identify key foulants deposited on the membrane surface during SWRO processes. Total dissolved solid concentrations were similar for all the source seawater and were in the range of 31,000–33,600 mg/L, and pH was between 7.8 and 8.0. Particulate concentration based on (SDI)₁₅ was higher (~6.3) for Tampa Bay seawater than for the other sources. The concentration of major ions in all the seawater sources was similar. Chloride and sodium were the major ions present in all sources. Among the divalent ions, magnesium concentration was significantly higher than calcium's. The concentration of major metals (iron, aluminum, nickel, and copper) was below detection limits in all the raw seawater sources. Boron concentrations varied between 2.4 and 4.7 mg/L for seawater in California. The boron concentration of Tampa Bay seawater was 3.8 mg/L.

Carbohydrate concentration of Tampa Bay seawater was higher than for seawater from Carlsbad, West Basin, and South Bay. Total carbohydrate (monomeric and polymeric) concentration for Tampa Bay seawater was ~8.5 mg/L as glucose. Also, TOC concentration was highest for Tampa Bay (~2.5 mg/L). TOC concentrations for all the other sources were below the lowest detection limit. To determine algal concentration in the source seawater, chlorophyll *a* was measured. Chlorophyll *a* concentrations were below detection limits (< 2 µg/L) for all the source waters.

Influence of membrane type and seawater source on organic fouling behavior

Membranes used for this study included DowFilmtec SW30HR, Hydranautics SWC4, and Saehan SR. DowFilmtec SW30HR and Saehan SR membranes were relatively smooth (RMS roughness ~ 78 nm) when compared to Hydranautics SWC4 (RMS roughness ~ 150 nm). DowFilmtec SW30HR was relatively hydrophilic ($\Delta G^{CO} > 0$) when compared to Saehan SR and Hydranautics SWC4 membranes ($\Delta G^{CO} < 0$). Streaming potential measurements were not significantly different at high ionic strengths (> 100 mM) for all three model membranes.

When different seawater sources were used, no significant difference in normalized specific flux was observed for Carlsbad, West Basin, and Tampa Bay seawaters during bench-scale RO experiments conducted with a Hydranautics SWC4 membrane. Although a significant decrease in specific flux was not observed during the bench-scale study, an autopsy of membrane coupons using ATR-FTIR, EDS, and imaging techniques revealed the presence of a foulant layer on the membrane surface. From SEM images, it was evident that the deposition of foulant was nonuniform on the membrane surface, which justifies the minimal decline in specific flux.

When different membrane types were compared for fouling propensity, relatively hydrophilic and smoother membranes (DowFilmtec SW30HR) exhibited slightly lower fouling potential than hydrophobic and rough membranes (Hydranautics SWC4). To study the influence of algal blooms, *H. pygmaea* cells were cultured and used in RO bench-scale experiments. During this study, no substantial difference in fouling behavior was observed when *H. pygmaea* algal spikes were used for studying influence of membrane properties on fouling. Because of the multilayer deposition and high concentration of AOM released from algal cell shearing, the effect of membrane properties on fouling characteristics was masked.

When AOM was used without any pretreatment of feed water, a gel layer was formed on the membrane surface. But with pre-MF, nonuniform deposition occurred on the membrane surface. Hence, pre-MF reduced the AOM content. Although a minimal decline in specific flux of the SWRO membrane was noticed with pre-MF, deposition of foulant was evident from autopsy techniques.

Identification of major organic foulants in seawater

Bench-scale RO experiments with various seawater sources and an autopsy performed on the fouled membrane coupon revealed the presence of polysaccharide-like material deposition on the membranes for all the seawater sources tested in this study. For all the seawater sources tested, absorbance spectra at 890 to 1050, 1620 to 1680, and 3000 to 3600 cm^{-1} were dominant. Pilot plant SWRO membrane leaf operated on Carlsbad seawater also revealed the presence of polysaccharide-like material, similar to bench-scale results. A thick slimy layer was visible on the pilot-scale membrane. In addition to the presence of polysaccharide-like material found on the pilot-scale membrane, additionally peaks at 1540 and 1640 cm^{-1} were noticed. The peaks were representative of amide-I and amide-II stretching prevalent in proteins. Iron was also identified on membrane coupons from both bench- and pilot-scale studies. Presence of iron revealed corrosion occurring both in the bench- and pilot-scale equipment.

Limitations of bench-scale experiments and characterization techniques

The bench-scale testing protocol must be combined with the various analytical, characterizations, and autopsy techniques to obtain meaningful results on organic fouling behavior in SWRO processes. The methods described in this study can be used as an early warning sign for determining only organic fouling of SWRO membranes. Other types of fouling such as biological fouling cannot be detected by the methods and procedures developed in this study. The bench-scale experiments and autopsy techniques as described in this study can be used to determine the nature of organic foulant occurring during normal operational periods as well as during algal blooms. However, seawater sampling during the various events needs to be undertaken and bench-scale experiments performed to compare results. Performing bench-scale experiments with seawater also can lead to problems due to

deposition of corrosion products on the membranes. It is essential that high-quality stainless steel equipment and parts are used while performing SWRO coupon tests. Proper protocol (as described in Appendix A) needs to be followed to obtain unbiased results.

4.2 RECOMMENDED FUTURE WORK

Because the bench-scale RO experiments were performed in this study for only 24 h, biofilm formation on the membrane surface was not noticed. In order to determine the biofouling potential of a particular seawater source, bench-scale experiments need to be modified accounting for time span of biofouling, microorganism type and metabolism, nutrient loading, etc. Organic deposition leads to the formation of conditioning films on the membrane surface and can influence subsequent biofilm formation. Hence, further studies are necessary to determine the influence of organic fouling on microbial adhesion in seawater systems. Future studies could also focus on understanding the structure of foulant layers formed. Because polysaccharides are predominantly deposited on the membrane surface, formation of a gel layer could be occurring because of preferential interaction between divalent cations and negatively charged functional groups on the polysaccharide molecule. The strength of adhesion between the polysaccharide-like material and the membrane surface also is not known. Depending on the type of membrane material used, the efficacy of cleaning the membrane and removing the foulant layer needs to be determined.

4.3 PRACTICAL ASPECTS OF THE STUDY

The techniques and methods used in this study can be used prior to the operation of a pilot-scale process in order to access the nature of foulant material that would preferentially deposit on the membrane surface. Because of the brevity of operation of bench-scale studies, they cannot be used as a substitute for pilot testing. The determination of the nature of the foulant being deposited on the membrane can be used to optimize the operating conditions during pilot-scale testing. For example, when a substantial amount of organic matter deposits during bench-scale coupon tests, causing a substantial decrease in the specific flux, a lower operating flux can be recommended for pilot-scale operations. Also, based on the nature of foulant material detected from the bench-scale testing, efficient cleaning chemicals specific to the foulant can be recommended for pilot-scale tests. It is important to combine the bench scale with the various analytical, characterization, and autopsy techniques to obtain meaningful results on organic fouling behavior in SWRO processes. The methods described in this study can be used as an early indication for determining only organic fouling of SWRO membranes. Other types of fouling such as biological fouling cannot be detected by the methods and procedures developed in this study. An understanding of the nature of foulant will facilitate cost-effective and optimal design/operation of pretreatment and the overall SWRO process.

References

- Adham, S.; Fane, A. G. *Report on Crossflow Sampler Fouling Index*; Report No. 06-ER-002; National Water Research Institute: Fountain Valley, CA, 2008.
- Al-Ahmad, M.; Aleem, F. A.; Mutiri, A.; Ubaisy, A. Biofouling in RO membrane systems, part 1: fundamentals and control. *Desalination* **2000**, *132*, 173–179.
- Allredge, A. L.; Passow, P. T.; Logan, B. E. The abundance and significance of a class of large, transparent organic particles in the ocean. *Deep Sea Res.* **1993**, *40*, 1131–1140.
- Brehant, A.; Bonnelye, P. V.; Perez, M. Comparison of MF/UF pretreatment with conventional filtration prior to RO membranes for surface seawater desalination. *Desalination* **2002**, *144*, 353–360.
- Brant, J.; Childress, A. Assessing short-range membrane-colloid interactions using surface energetics. *J. Membr. Sci.* **2002**, *203*, 257–273.
- Characklis, W. G.; Marshall, K. C. *Biofilms*; John Wiley and Sons, Inc.: Hoboken, NJ, 1990.
- Childress, A.; Elimelech, M. Effect of solution chemistry on the surface charge of polymeric reverse osmosis and nanofiltration membranes. *J. Membr. Sci.* **1996**, *119*, 253–268.
- Elimelech, M.; Zhu, X.; Childress, A.; Hong, S. Role of membrane surface morphology in colloidal fouling of cellulose acetate and composite aromatic polyamide reverse osmosis membranes. *J. Membr. Sci.* **1997**, *127* (1)101–109.
- Flemming, H. C.; Schaule, G. Biofouling on membrane—a microbiological approach. *Desalination* **1988**, *70* (1–3), 95–119.
- Flemming, H. C.; Schaule, G.; Griebe, T.; Schmitt, J.; Tamachkiarowa, A. Biofouling—the Achilles heel of membrane processes. *Desalination* **1997**, *113*, 215–225.
- Ghani, A.; Al-Rasheed, R.; Javeed, M. A. Studies on organic foulants in the seawater feed for reverse osmosis plants of SWCC. *Desalination* **2000**, *132*, 217–232.
- Glueckstern, P.; Priel, M.; Wilf, M. Field evaluation of capillary UF technology as a pretreatment for large seawater RO systems. *Desalination* **2002**, *147*, 55–62.
- Grasso, D. A review of non-DLVO interactions in environmental colloidal systems. *Rev Environ Sci Biotechnol* **2002**, *1*, 17–38.
- Hoek, E. M. V.; Bhattacharjee, S.; Elimelech, M. Effect of membrane surface roughness on colloid-membrane DLVO interactions. *Langmuir* **2003**, *19*, 4836–4847.
- Isaias, N. P. Experience in reverse osmosis pretreatment. *Desalination* **2001**, *139*, 57–64.
- Jarusutthirak, C.; Amy, G. Fouling characteristics of wastewater effluent organic matter (EfOM) isolates on NF and UF membranes. *Desalination* **2002**, *145*, 247–255.
- Kumar, M.; Adham, S.; Pearce, W. R. Investigation of seawater reverse osmosis fouling and its relationship to pretreatment type. *Environ. Sci. Technol.* **2006**, *40*, 2037–2044.
- Leparc, J.; Rapenne, S.; Courties, C.; Lebaron, P.; Croue, J. P.; Jacquemet, V.; Turner, G. Water quality and performance evaluation at seawater reverse osmosis plants through the use of advanced analytical tools. *Desalination* **2007**, *203*, 243–255.

- Li, Q.; Xu, Z.; Pinnau, I. Fouling of reverse osmosis membranes by biopolymers in wastewater secondary effluent: role of membrane surface properties and initial permeate flux. *J. Membr. Sci.* **2007**, *290*, 173–181.
- Lowry, O. H.; Rosebrough, N. J.; Farr, A. L.; Randall, R. J. Protein measurement with the Folin phenol reagent. *J. Biol. Chem.* **1951**, *193*, 265–275.
- Lozier, J. C.; Reynolds, T.; Frenkel, V.; Castle, R.; Sellier, P. Using Autopsy Techniques to Understand Differences in SWRO Membrane Fouling—Conventional vs. MF/UF Pretreatment Impacts. *Proceedings of the 2007 Membrane Technology Conference*, Tampa, FL, 2007; AWWA: Denver, CO, 2007.
- Myklestad, S. M.; Skanoy, E.; Hestmann, S. A sensitive and rapid method for analysis of dissolved mono- and polysaccharides in seawater. *Mar. Chem.* **1997**, *56*, 279–286.
- Reiss, C. R.; Robert, C.; Dietrich, J.; Mody, A. *Pretreatment and Design Considerations for Large-Scale Seawater Facilities*; DWPR Report No. 137; U.S. Bureau of Reclamation, U.S. Government Printing Office: Washington, DC, 2008.
- Saeed, M. O.; Jamaluddin, A. T.; Tisan, I. A.; Lawrence, D. A.; Al-Amri, M. M.; Chida, K. Biofouling in a seawater reverse osmosis plant on the Red Sea coast, Saudi Arabia. *Desalination* **2000**, *128*, 177–190.
- Schneider, R. P. Conditioning film-induced modification of substratum physicochemistry—analysis by contact angles. *J. Colloid Interface Sci.* **1996**, *182*, 204–214.
- Shimadzu Corporation. Application Note: TOC Determination in Seawater. http://www.shimadzu-france.com/enews/mars09/files/Shimadzu_TOC.pdf (accessed Nov 2010).
- Shon, H. K.; Vigneswaran, S.; Cho, J. Comparison of physico-chemical pretreatment methods to seawater reverse osmosis: detailed analyses of molecular weight distribution of organic matter in initial stage. *J. Membr. Sci.* **2008**, *320*, 151–158.
- Teng, C. K.; Hawlader, M. N. A.; Malek, A. An experiment with different pretreatment methods. *Desalination* **2003**, *156*, 51–58.
- van Oss, C. J. Acid–base interfacial interactions in aqueous media. *Colloids Surf., A* **1993**, *78*, 1–49.
- Veza, J. M.; Ortiz, M.; Sathwani, J. J.; Gonzalez, J. E.; Santana, F. J. Measurement of biofouling in seawater: some practical tests. *Desalination* **2008**, *220*, 326–334.
- Villacorte, L. O., Kennedy, M. D., Amy, G. L., Schippers, J. C. The fate of transparent exopolymer particles (TEP) in integrated membrane systems: removal through pretreatment processes and deposition on reverse osmosis membranes. *Water Res.* **2009**, *43*, 5039–5052.
- Visvanathan, C.; Boonthanon, N.; Sathasivan, A.; Jegatheesan, V. Pretreatment of seawater for biodegradable organic content removal using membrane bioreactor. *Desalination* **2002**, *153*, 133–140.
- Voutchkov, N. Desalination—water for the next generation. *Filtr. Sep.* **2005**, *42*, 14–25.
- Vrijenhoek, E. M.; Hong, S.; Elimelech, M. Influence of membrane surface properties on initial rate of colloidal fouling of reverse osmosis and nanofiltration membranes. *J. Membr. Sci.* **2001**, *188*, 115–128.

- Watkins, G. S.; Gupta, H. B. A comparative study of organic fouling in hollow fiber and spiral wound membranes. *Desalination* **1987**, *66*, 299.
- Wilf, M.; Klinko, K. Effective new pretreatment for seawater reverse osmosis systems. *Desalination* **1998**, *117*, 323–331.
- Winters, H. Control of organic fouling at two seawater reverse osmosis plants. *Desalination* **1987**, *66*, 319–325.
- Winters, H. *Biofouling Status of the Saline Water Conversion Corporation (SWCC): Reverse Osmosis (RO) Plants in the Kingdom of Saudi Arabia*; Consultancy Report; Riyadh, Saudi Arabia, 1994.
- Xu, P.; Drewes, J. E.; Kim, T.; Bellona, C.; Amy, G. Effect of membrane fouling on transport of organic contaminants in NF/RO membrane applications. *J. Membr. Sci.* **2006**, *279*, 165–175.

Appendix A

Procedure for Bench Scale RO Membrane Test

Membrane coupon preparation

- Cut coupons from flat sheets or spiral-wound modules.
- Store coupons in DI water at 4 °C, replacing water regularly to minimize bacterial or fungal growth.

RO unit cleaning

- With the membrane cell removed from the system, run a 7% phosphoric acid solution through the system in recycle mode for 10 min.
- Rinse thoroughly with DI water.
- Test the conductivity of water in the system to ensure that acid has been thoroughly rinsed away.

Bench-scale RO unit setup

- Follow diagram in Figure 2.4 RO setup.
- Calibrate conductivity meters. Use a 50-mS/cm standard for measuring feed conductivity and 0.447 mS/cm for permeate conductivity.
- Before placing membrane in the system, run at 1000 psi to ensure that pump pulsation does not occur.

Compaction run

- Replace DI water in the system with a sodium chloride solution at 32 g/L (0.55 M; conductivity near 50 mS/cm). A volume of at least 8 L is recommended, depending on the tubing and tanks used.
- Place membrane coupon in test cell and pressurize to 1200 psi.
- Start flow through the system and begin computerized collection of pressure, flux, temperature, and conductivity data.
- With the system running at a set pump speed, tighten the concentrate valve to increase pressure. Increase the pressure slowly (for 1 or 2 min) until it reaches 1000 psi. The crossflow rate in the system is typically about 800 mL/min, giving a nominal crossflow velocity of about 50 cm/s. At 1000 psi, the flux for a 32-g/L NaCl solution is usually about 30 lmh.
- Monitor the system for at least 30 min and ensure that proper rejection (typically at least 98%, often higher than 99%) is being achieved. Also ensure that temperature is kept constant (20 °C is typical).
- Run at constant 1000-psi pressure in recycle mode (permeate returned to feed tank) for 24 h and observe flux decline due to compaction.
- Monitor the feed-tank conductivity over time, ensuring that it remains constant.

Fouling test

- Shut down the system from the compaction run. Note that the membrane will begin to relax as soon as the pressure is turned off, so it is important to make the switch from compaction solution to seawater solution as quickly as possible.
- Remove most of the water in the system down to the pump level, but do not run air through the pump.
- Sample the seawater to be tested and store it for later water quality analyses.

- For seawater testing it is advisable to use as much volume as possible. Twenty liters is typically used in our lab.
- Waste at least 1 L of seawater through the system to flush out the NaCl solution.
- Restart the system at the same flow rate used for the compaction run.
- Start computer datum collection and bring pressure up steadily for 1 or 2 min until it reaches 1000 psi.
- Record the permeate conductivity regularly, but especially toward the beginning. Ensure that proper rejection (at least 98%) is being achieved.
- Run at constant 1000-psi pressure in recycle mode for 24 h.
- Monitor the feed-tank conductivity over time, ensuring that it remains constant.
- Sample the feed tank at the end of the run for water quality analyses.
- Sample the permeate if permeate quality parameters are to be measured.

Shutdown

- After the 24-h fouling run, turn off the system.
- Remove the membrane from the testing cell, being careful not to disturb the foulant layer.
- Store the membrane at 4 °C and allow it to dry overnight.
- After the overnight drying, take a picture of the membrane (a desktop scanner is typically used); then place it in a desiccator for long-term storage and future analyses.
- Flush DI water through the RO unit to remove salts.

Advancing the Science of Water Reuse and Desalination



1199 North Fairfax Street, Suite 410

Alexandria, VA 22314 USA

(703) 548-0880

Fax (703) 548-5085

E-mail: Foundation@WateReuse.org

www.WateReuse.org/Foundation